

Fabian Böhmer  
NTNU  
Norwegian University of  
Science and Technology  
Faculty of Engineering  
Department of Energy and Process Engineering

Fabian Böhmer

# Design of a PCM-based heat storage unit for the ZEB Flexible Laboratory

June 2019



Norwegian University of  
Science and Technology

# Design of a PCM-based heat storage unit for the ZEB Flexible Laboratory

**Fabian Bøhmer**

Master's Thesis in Mechanical Engineering

Submission date: June 2019

Supervisor: Erling Næss, EPT

Co-supervisor: Alexis Sevault, SINTEF Energy Research

Norwegian University of Science and Technology  
Department of Energy and Process Engineering

---

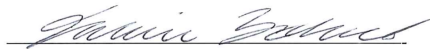
# Preface

This master's thesis is the final work of the 5-year "Mechanical Engineer" programme at the Norwegian University of Science and Technology. The thesis was written during the spring of 2019 at the Department of Energy and Process Engineering in collaboration with SINTEF Energy Research.

The title of the thesis is: Assisting the design of a PCM-based heat storage unit for heating system in buildings. It involves literature review and the development of a simulation model to design a heat storage unit to be installed in an office building in Trondheim.

I want to thank my supervisor Erling Næss, Professor at the Department of Energy and Process Engineering, for giving me the opportunity to write this master's thesis and for his excellent guidance throughout the process.

A special thanks to Alexis Sevault, PhD Research Scientist at SINTEF Energy for bringing me on board and up to date on the ZEB Flexible Laboratory project. The support, responsibility and answers during countless office drop-ins have been crucial for the completion of this master's thesis.



Fabian Böhmer  
Trondheim, 11.06.2019

---

# Abstract

The ZEB Flexible Laboratory project, coordinated by SINTEF and NTNU, aims at building a ZEB (Zero Energy Building) in Trondheim in 2019, to act as both an office building and a laboratory. A latent heat storage (LHS) unit is to be implemented and tested in the building to increase the energy performance by the use of phase change materials (PCMs).

The purpose of the master's thesis was to assist the design of a compact and effective LHS system for the ZEB Flexible Laboratory. During periods of peak heat demand, through energy storage, the LHS system will help balance the gap between the heat demand of the building and the heat output of the buildings main source of heat, a ground-source heat pump. The boundary conditions for the system have been defined and a preliminary LHS concept has been designed. Through the study of literature and the construction of a dynamic PCM heat exchanger model in Dymola, the transient course of energy absorption/release of a latent heat storage was investigated. By simulating charging and discharging processes of a LHS unit model, critical design parameters that affect the melting and solidification times are identified to help design a well functional LHS unit applicable for the buildings properties and local conditions.

Results showed that a plate fin-and-tube LHS design was able to store sufficient amounts of energy to assist the heat pump during cold periods with excessive heat demand. A commercial PCM was selected, CT37, suitable for the thermal design properties of the heating system. A LHS design consisting of 225 copper pipes running through aluminum plate fins with PCM filling the void was able to obtain adequate heat transfer rates to ensure the achievement of comfortable indoor conditions during cold periods. A fin pitch of 2 cm and a fin thickness of 1 mm proved to enhance the heat transfer in the LHS unit enough for the unit to be able to be fully charged during the night ( $\sim 11$  hours) when heat demand typically is low. Pressure drop calculations were performed for the heat transfer fluid (HTF) through the LHS unit to find the required pump power to compensate for pressure drop for different pipe flow configurations through the system. A configuration of 45 separate flows, resulted in a pressure drop of 0.495 bar, requiring a pump power of 0.3 kW including a safety factor.

---

# Sammendrag

Prosjektet ZEB Flexible Laboratory, koordinert av SINTEF og NTNU, har som mål å bygge et ZEB (Zero Energy Building) i Trondheim i 2019, som skal fungere som både kontorbygg og laboratorium. En latent varmelagringsenhet skal implementeres og testes for å øke energiytelsen til bygget ved å utnytte latent varme i ett faseovergangs-material.

Hensikten med denne masteroppgaven er å bidra til utformingen av et kompakt og effektivt varmelagringsenhet for ZEB Flexible Laboratory. I perioder med høyt varmebehov, gjennom energilagring, vil varmelagringsenheten bidra til å balansere differansen mellom bygningens varmebehov og varmekilde, en bergvarmepumpe. Grensebetingelsene for enheten er definert og et foreløpig varmelagringskonsept er utformet. Ved å studere tidligere arbeid og gjennom å bygge en dynamisk varmelagringsenhetmodell i Dymola, vil den transiente utviklingen under energiabsorpsjon/-frigjøring av latent varme undersøkes. Ved å simulere ladings og utladningsprosesser av en latent varmelagringsenhet, er målet å identifiseres kritiske design parametere som påvirker smelte- og størkningsstider. For så å kunne bruke resultatene til å designe en velfungerende enhet egnet til bygningens bruk og lokale forhold.

Resultatene viste at en varmelagringsenhet bestående av platefinner og rør var i stand til å lagre tilstrekkelig mengde varme, til å supplere varmepumpen under perioder med høyt varmebehov. En kommersiell PCM har blitt valgt, CT37, med termiske egenskaper godt egnet for byggets oppvarmingssystem. En latent varmeenhet bestående av 225 kobberør og aluminiumplatefinner med fasematerial i tomrommet mellom, er i stand til å oppnå tilstrekkelig varmeoverføringshastighet til å sikre komfortable forhold i bygget under kalde perioder. En finneavstand på 2 cm og en finnetykkelse på 1 mm viste seg å øke varmeoverføringen nok til at enheten kunne bli fulladet i løpet av natten (~ 11 timer), da varmebehovet til bygningen er lavt. Trykkfallsberegninger ble utført for vannet gjennom varmelagringsenheten for å finne den nødvendige pumpeeffekten for å kompensere for trykkfall for forskjellige rørstrømskonfigurasjoner gjennom systemet. En konfigurasjon på 45 separate vannstrømmer, resulterte i et trykkfall på 0,495 bar, hvilket krever en pumpeeffekt på 0.3 kW, inkludert en sikkerhetsfaktor for eventuelt høyere trykkfall.

# Table of Contents

<b>Preface</b>	<b>i</b>
<b>Abstract</b>	<b>ii</b>
<b>Sammendrag</b>	<b>iii</b>
<b>Table of Contents</b>	<b>iv</b>
<b>List of Tables</b>	<b>v</b>
<b>List of Figures</b>	<b>vii</b>
<b>Nomenclature</b>	<b>viii</b>
<b>1 Introduction</b>	<b>1</b>
1.1 Background . . . . .	1
1.2 Objective . . . . .	3
1.3 Limitations . . . . .	3
1.4 Report Structure . . . . .	3
<b>2 Theory</b>	<b>5</b>
2.1 Thermal Energy Storage . . . . .	5
2.1.1 Sensible Heat Storage . . . . .	6
2.1.2 Latent Heat Storage . . . . .	6
2.2 Phase Change Materials . . . . .	6
2.2.1 PCM Properties . . . . .	7
2.2.2 PCM Classification . . . . .	8
2.2.3 PCM Selection . . . . .	9
<b>3 Heating systems for buildings</b>	<b>11</b>
3.1 Design of Centralized Heating Systems . . . . .	11
3.2 Design of PCM-based Heat or Cold Storage Units . . . . .	12
3.2.1 General . . . . .	12
3.2.2 Design Criteria . . . . .	14
3.2.3 PCM Containers and Encapsulation . . . . .	15
3.2.4 Heat Transfer Enhancement . . . . .	18
3.2.5 LHS Integration with Heat Pump . . . . .	22

---

<b>4</b>	<b>Case Study:</b>	<b>24</b>
	<b>ZEB Flexible Laboratory</b>	<b>24</b>
4.1	General . . . . .	24
4.2	Latent Heat Storage Unit . . . . .	25
4.2.1	Unit Integration . . . . .	26
4.2.2	Control Strategy . . . . .	27
4.2.3	PCM Selection . . . . .	28
4.2.4	Unit Design . . . . .	29
4.2.5	HTF Distribution and Pump Power . . . . .	31
4.2.6	Other Considerations . . . . .	32
4.3	Building Heat Demand . . . . .	32
<b>5</b>	<b>Dynamic System Model</b>	<b>35</b>
5.1	Model Description . . . . .	35
5.2	Model Assumptions . . . . .	36
5.3	Input Parameters . . . . .	37
5.4	Discretization . . . . .	38
5.5	Model output . . . . .	40
5.6	Validification of Model . . . . .	40
<b>6</b>	<b>Results and Discussion</b>	<b>43</b>
6.1	Variable Fin Pitch . . . . .	43
6.2	Variable Mass Flow . . . . .	47
6.3	Variable Fin Thickness . . . . .	49
6.4	Variable Pipe Flow Configuration . . . . .	50
<b>7</b>	<b>Conclusion</b>	<b>53</b>
7.1	Further work . . . . .	54
	<b>Bibliography</b>	<b>54</b>
	<b>Appendices</b>	<b>59</b>
A	Validation correspondence with TLK-Thermo GmbH . . . . .	59
B	Scientific publication . . . . .	60
C	Matlab script for heat transfer coefficient calculations . . . . .	68
D	Matlab script for pressure drop calculations . . . . .	69
E	Matlab script for LHS unit heat loss . . . . .	70

---

# List of Tables

3.1	Selection of commercially available PCMs. . . . .	15
4.1	Commercial PCMs qualified for the LHS unit. . . . .	28
4.2	General design parameters of LHS-1. . . . .	30
4.3	Required pump power for different LHS pipe configurations . . . . .	32
4.4	LHS system requirements for different heat pump power outputs. . . . .	34
5.1	Parameters for the PCM heat exchanger model. . . . .	37
5.2	Parameters for initialization of the PCM heat exchanger model. . . . .	37
6.1	Base case heat exchanger parameters. . . . .	43



# List of Figures

1.1	Illustratuion of thermal energy storage implemented in centralized heating.	1
2.1	Phase change diagram where temperature is plotted against heat added. Subscripts $m$ and $e$ denotes melting and evaporation [40]. . . . .	5
2.2	Classification of PCMs. . . . .	8
3.1	Illustration of heat demand throughout a day. . . . .	12
3.2	Different ways of integrating TES systems in a building [38]. . . . .	13
3.3	Number of published articles on the topic "PCM heat storage" since 2000. Source: Web of Science. . . . .	14
3.4	Classification of PCM containers. . . . .	16
3.5	Illustration of parallell and co-current flow in a shell and tube system. . .	18
3.6	Different fin geometry for increased HTE in tubes. . . . .	18
3.7	Melting time (a) and solidification time (b) for different mass flow rates and fin pitches [34]. . . . .	19
3.8	Heat transfer coefficient between HTF and PCM for different inlet temperatures [9]. . . . .	20
3.9	Heat transfer enhancement methods [43]. . . . .	21
3.10	Solidification time for different HTE methods [43]. . . . .	22
4.1	ZEB Flexible Labratory [22]. . . . .	25
4.2	Hydronic heating system diagram for ZEB Flex Labratory. . . . .	26
4.3	Process diagram of the centralized heating system illustrating the LHS units.	27
4.4	Control strategy for LHS-1. . . . .	28
4.5	Heat flow absorbed and released by a sample of CT37 for 10 melting/solidification cycles measured with DSC. . . . .	29
4.6	Illustration of LHS unit. . . . .	30
4.7	Heat loss through LHS unit container wall for different insulation thickness. Assuming no loss through radiation. See Appendix E for thermal properties of tank components. . . . .	31
4.8	Illustration of different pipe flow configurations for the LHS unit. . . . .	32
4.9	Heat demand for the coldest week in January. . . . .	33
4.10	Heat demand for the coldest 3-week period in January. . . . .	34
5.1	PCM heat exchanger model in Dymola. . . . .	36
5.2	Illustration of fin and tube heat exchanger geometry. . . . .	38
5.3	Internal structure of PCM heat exchanger model. . . . .	39
5.4	Discretization of the heat exchanger model: Axially along the heat exchanger (a) and radially (b). . . . .	39
5.5	Simulation and experimental data for discharge of PCM TES. . . . .	41

---

5.6	PCM temperature development during charging/discharging of a fin and tube TES system. . . . .	42
6.1	Temperature of HTF at inlet and outlet, PCM average temperature during charging. . . . .	44
6.2	Heat flow from HTF to PCM and PCM liquid fraction during charging. . .	45
6.3	Temperature of HTF at inlet and outlet, PCM average temperature during discharging. . . . .	46
6.4	Heat flow from HTF to PCM and PCM liquid fraction during discharging. .	47
6.5	Temperature of HTF at inlet and outlet, PCM average temperature during charging. . . . .	48
6.6	Temperature of HTF at inlet and outlet, PCM average temperature during discharging. . . . .	48
6.7	Average PCM temperature and total amount of PCM in LHS unit during a charging cycle. . . . .	49
6.8	Average PCM temperature for an increasing number of separate flows during a charging cycle. . . . .	51
6.9	Calculated heat transfer coefficient for HTF [Appendix C]. . . . .	51
6.10	Pressure drop for HTF [Appendix D]. . . . .	52

# Nomenclature

## Symbols

$\Delta t_{cycle}$	Duration of heating cycle	[s]
$\overline{\dot{q}}''_{hot}$	Average heat flux	$[\frac{W}{m^2}]$
$a_m$	Fraction melted	
$Bi$	Biot number	
$c_p$	Specific heat	$[\frac{J}{kg \cdot K}]$
$e_v$	Volumetric energy density	$[\frac{J}{m^3}]$
$k$	Thermal conductivity	$[\frac{W}{m \cdot K}]$
$m$	Mass	[kg]
$Q$	Heat energy	[J]
$Re$	Reynolds number	
$T$	Temperature	[K]
$H_f$	Heat of fusion	$[\frac{J}{kg}]$

## Subscripts

$amb$	Ambient
$e$	Effective
$f$	Final
$i$	Initial
$l$	Liquid
$m$	Melting
$s$	Solid

## Abbreviations

---

<i>DSC</i>	Differential scanning calorimetry
<i>HDPE</i>	High-density polyethylene
<i>HTE</i>	Heat transfer enhancement
<i>HTF</i>	Heat transfer fluid
<i>LHS</i>	Latent heat storage
<i>PCM</i>	Phase change materials
<i>SCOP</i>	Seasonal coefficient of performance
<i>SF</i>	Number of separate flows
<i>SHS</i>	Sensible heat storage
<i>TES</i>	Thermal energy storage
<i>ZEB</i>	Zero energy building

# 1 — Introduction

## 1.1 Background

A transition to energy efficient buildings is one of the most economically viable options to reduce greenhouse gas emissions and reduce energy consumption. Buildings (households and service activities) represent 49 % of the total electricity consumption in Norway [41]. Thermal energy storage (TES) systems can be implemented in a buildings heating system to help overcome the lack of concurrence between the energy supply and demand. This prevents unnecessary oversizing of expensive production equipment by smoothing peak load. By operating heat pumps under more efficient conditions, energy consumption can be greatly reduced.

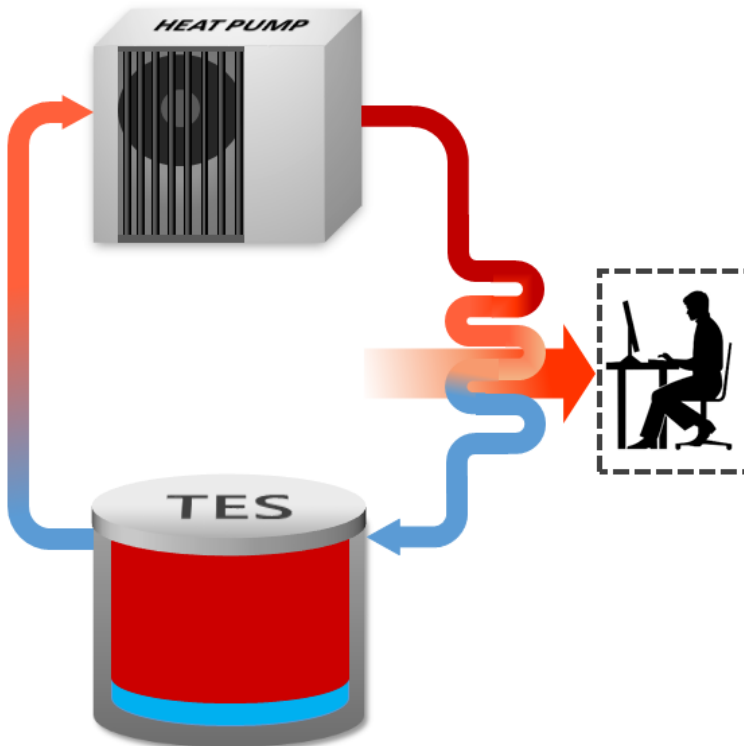


**Figure 1.1:** Illustratuion of thermal energy storage implemented in centralized heating.

By exploiting the phase change of a material, its latent heat can be utilized to achieve much higher energy storage density, compared to sensible heat storage. In a latent heat system, thermal energy can be stored or released due to the process of phase transition of a material occurring at close to isothermal conditions. A change in state from solid to liquid (melting) or liquid to solid (solidification) is fundamental in enabling thermal energy storage in a phase change material (PCM). The low thermal conductivity of the cost-effective storage materials is the main challenge in the development of effective LHS systems. Thus, a comprehensive design is needed to obtain a working system where the PCM thermal properties matches the dynamic use of the building. There are several ways to incorporate PCM technology for heat storage purposes in building environments. Passive systems include encapsulation of PCM into building materials such as concrete, ceiling boards, floors and gypsum boards [6]. Active systems ensures a higher degree of control over the indoor environmental conditions and improves the method of storing heat energy [3]. One way to integrate an active system is by coupling a LHS system to a heat pump in a hydronic heating system. The LHS system can store and release energy at periods of fluctuating heat demand to supply the heat pump with more balanced inlet temperatures. Ultimately leading to more efficient operation of the heat pump which can reduce overall energy consumption and increase energy efficiency. Research on such a system has been carried out experimentally [44] [15], but there are few full-scale systems installed for building heating purposes. It is then crucial to design, build and implement a fully functional system to test the potential of a LHS system incorporated for heating purposes. During the spring of 2019, a collaboration between NTNU and SINTEF aims to build a Zero Emission Building, the ZEB Flexible Laboratory, in Trondheim. It will be an office building and a laboratory where innovative and potentially energy efficient technical solutions can be tested. One of them will be a LHS unit integrated in the buildings centralized heating system.

## 1.2 Objective

The purpose of the master's thesis is to assist the design of a compact and effective LHS system to be built up and integrated in the upcoming ZEB Flexible Laboratory. The boundary conditions for the system have been defined and a preliminary LHS concept has been designed. The following tasks will be completed:

1. Literature review focusing on:
  - General principles of heat storage using PCMs
  - General design of centralized heating systems for buildings
  - Similar design of PCM-based heat or cold storage units
2. Assist main design of heat storage unit
  - Selection of best available PCM and manufacturer
  - Dimensioning of container, water pump, water distribution in container
  - Proposal for instrumentation equipment and control strategies
3. Evaluation of heat transfer rates for charge and discharge through numerical modeling
4. Participate in the writing of a peer-reviewed scientific publication.

## 1.3 Limitations

The objective of the master's thesis is to assist in the design of a heat storage unit. To obtain realistic results from dynamic system modeling, it would be desirable with design data for the hydronic heating system to use as input data for the constructed dynamic model. Due to delays in the design process of the ZEB Flexible Laboratory, hydronic heating system data such as mass flow rates, working fluid temperatures and heat pump capacities were not available. Therefore, data from early stage planning of the building are used for simulations and heat demand calculations.

## 1.4 Report Structure

- Chapter 2 - Presents the general theory about thermal energy storage and phase change materials.
- Chapter 3 - This chapter focuses on the general design of centralized heating system and PCM-based heat/cold storage units and studies/ work done on these topics.
- Chapter 4 - Presents the ZEB Flexible Laboratory and the requirements for the latent heat storage unit to be installed in the building.

- Chapter 5 - The dynamic model for transient simulation of the LHS unit is described and validated.
- Chapter 6 - Results from the dynamic model are presented and discussed in this chapter.
- Chapter 7 - The conclusion is given and recommendations for further work are given.



# 2 — Theory

This chapter will introduce the general theory about thermal energy storage (TES) and phase change materials (PCM)

## 2.1 Thermal Energy Storage

Thermal energy storage is the temporarily storage of thermal energy that can be used, at a later point, for heating or cooling under different conditions such as temperature, location or power [5]. By utilizing a TES system in a building, peak demand of energy can be reduced, total energy consumption can be reduced and overall system efficiency can be increased. TES can also help balance energy demand for a building on a time scale scoping from a daily to a yearly basis. TES systems are divided into three different types:

- Sensible heat storage
- Latent heat storage
- Thermochemical storage

Thermochemical storage will not be discussed further. Fig. 2.1 shows a phase diagram.

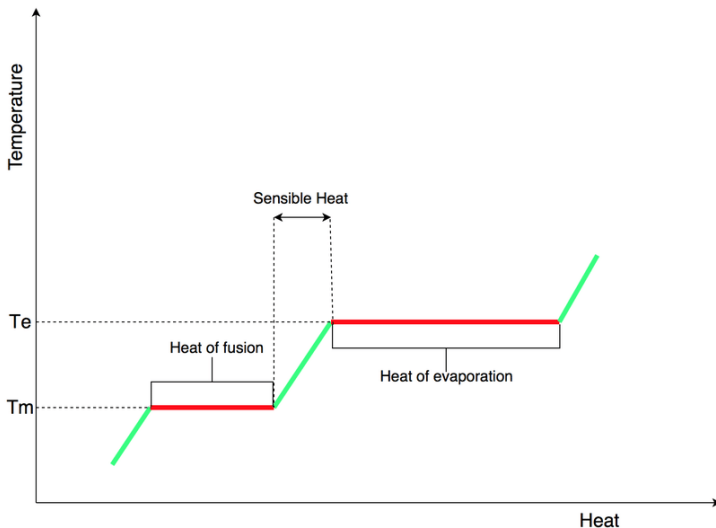


**Figure 2.1:** Phase change diagram where temperature is plotted against heat added. Subscripts  $m$  and  $e$  denotes melting and evaporation [40].

### 2.1.1 Sensible Heat Storage

Sensible heat storage (SHS) is storage of heat energy through the temperature change of a material. The storage material is typically a solid or a liquid. Every material has its advantages and disadvantages. By adding heat to a material, the temperature of the material is increased. The amount of heat stored in a material depends on the amount of storage material, the temperature difference between the material and its surroundings, and the heat capacity of the material. The amount of energy stored is described by Eq. (2.1):

$$Q = \int_{T_i}^{T_f} m \cdot C_p \cdot dT = m \cdot C_p \cdot \Delta T \quad (2.1)$$

where  $Q$  is the amount of heat energy [J] stored in the material,  $m$  is the mass amount [kg] of the storage material,  $C_p$  is the specific heat capacity of the storage material and  $\Delta T$  is the temperature change.

### 2.1.2 Latent Heat Storage

Latent heat storage (LHS) exploits the transition between phases of a material. Solid- liquid phase change is most often used, where the working principle for LHS is that when heat is applied to a material the phase changes from solid to liquid by storing the heat as latent heat of fusion. When the phase changes from liquid to gas, latent heat of vaporization is stored. During melting, heat is transferred to the material, storing large amounts of energy at a near constant temperature. For solid- solid phase change, heat is stored in the material during transformation from one crystalline to another. Compared to solid- liquid phase change, this yields smaller latent heat and smaller changes in material volume. Solid -solid LHS thus offers greater design flexibility with the absence of liquid and container requirements are less strict due to smaller volume changes. Solid- gas and liquid- gas phase change offers higher latent heat compared to solid-liquid transitions. But as the volume changes greatly during phase transitions, it is impracticable to use in thermal storage systems due to containment challenges. A great advantage with latent heat storage is its possibility to store large amounts of energy compared to SHS, because of its high energy density. For a given temperature range, 5-14 times more heat per volume can be stored as latent heat, compared to SHS. This results in smaller storage volumes [38]. The storage capacity of a LHS system with a PCM material is given by Eq. (2.2) [30]:

$$Q = \int_{T_i}^{T_m} m_s \cdot C_{p,s} \cdot dT + m \cdot a_m \cdot H_f + \int_{T_m}^{T_f} m_l \cdot C_{p,l} \cdot dT \quad (2.2)$$

## 2.2 Phase Change Materials

Materials that are used to store latent heat are called phase change materials (PCM). Water is probably the best known PCM and has been utilized for cold storage since early times.

Theoretically, every material is a PCM, because at some combinations of pressure and temperature every material will change its aggregate state. During this change of state, large amounts of heat can be stored or released as latent heat at close to constant temperature. Practical PCMs are materials that complete solid-liquid phase transition close to the operating temperature range of a selected thermal application [38]. The heat that is absorbed or released during the phase transition is called the latent heat of fusion, illustrated above in Fig. 2.1.

### 2.2.1 PCM Properties

The choice of PCM for an application always involves a compromise to some degree when it comes to the material properties. However it is most favourable with large high latent heat and high thermal conductivity. Oró et al. [30] conducted a review on a range of phase change materials for thermal energy storage applications and listed the following main characteristics required for a useful PCM:

- Thermophysical properties:
  - Phase change temperature range practical to the application
  - Considerable latent heat per unit of volume
  - Considerable sensible heat per unit of volume
  - Large thermal conductivity for both liquid and solid phase
  - Small density changes during phase transitions
  - Congruent phase change, i.e no segregation
  - Reproducible phase change without degradation of the phase change cycles
- Nucleation and crystal growth:
  - High nucleation rate to restrict subcooling of liquid during the solidification and to assure similar temperature for solidification and melting processes
  - High rate of crystal growth to assure sufficiently fast charging and discharging of PCM reservoir
- Chemical properties:
  - Reversible phase transition cycle
  - No degradation over time for phase transition cycles
  - Non corrosive properties to the construction/encapsulation properties
  - Non- toxic, non- flammable and non- explosive
- Economics and usability:
  - Availability and cost
  - Easy recycling and handling
  - Good environmental performance based on life cycle analysis

## 2.2.2 PCM Classification

The main categorization of PCMs is the differentiation between organic, inorganic, metallic and eutectic PCMs. Eutectics are defined generally as alloys or a composition of two or more components which melts and freezes congruently producing a mixture of the component crystals during crystallization. Figure 2.2 shows the categorization of PCMs:

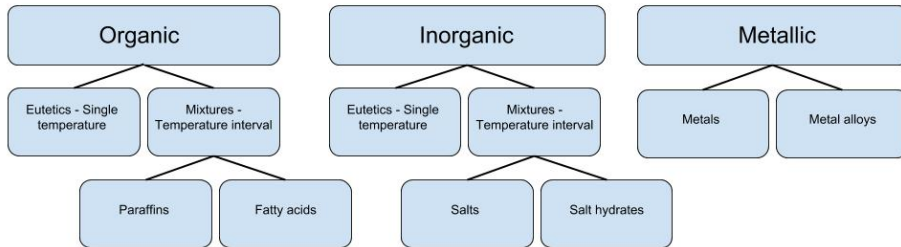


**Figure 2.2:** Classification of PCMs.

### 2.2.2.1 Organic PCMs

Organic PCMs are among the most commonly used PCMs, and are divided into paraffin and non-paraffin where we find the fatty acids. These PCMs include congruent melting, which means that melting and freezing can happen repeatedly without phase segregation or degradation of latent heat of fusion. These organic materials are usually non-corrosive and self nucleate, which means that crystallize with little or no supercooling [39]. Paraffins have melting temperatures in the range of 35 to 70 °C, which make them practical for thermal management in power electronics. On a cost consideration, only technical grade paraffins may be used as PCMs in LHS systems [39]. Fatty acids have lower melting temperatures than paraffins, and are used commonly in residential buildings for thermal comfort applications. However, fatty acids are costly, 2- 2.5 times greater than that of technical grade paraffins [39]. Organic PCMs have relatively high latent heats, but their thermal conductivity are usually low, typically around  $0.2 \text{ W}\cdot(\text{m}\cdot\text{K})^{-1}$ . This, combined with low densities and non-sharp phase transitions limits their application.

### 2.2.2.2 Inorganic PCMs

The main inorganic PCMs are salts, salt hydrates, aqueous solutions and water, which is the first PCM ever used to help cool materials. Salt hydrates are combinations of the components under inorganic salts and water molecules. Salt and salt hydrates typically have melting temperatures in the range of 10 to 900 °C. Organic PCMs are preferred in the lower temperature range, but salts and salt hydrates are more common to use in the high temperature range. These PCMs have sharp phase transitions at the melting temperature, similar latent heats but higher thermal conductivity compared to organic PCMs. Inorganic PCMs have higher densities and smaller changes in volume during phase transition in contrast to organic PCMs. Furthermore, the high storage density of salt hydrates can be difficult to maintain and will decrease over time. This leads to a degradation of their

storage efficiency. There is a tendency for supercooling for hydrated salts, where the salt hydrates starts to solidify at a temperature below the actual melting temperature. This challenge can be solved by adding nucleating agents to the PCM.

### 2.2.2.3 Metallic PCMs

Metals and metallic alloys can be used for PCM applications. Gallium and cesium are suitable to use for low- medium temperature applications, with a melting temperature of  $\sim 30^\circ\text{C}$ . Indium, tin and bismuth with melting temperatures from  $100\text{-}200^\circ\text{C}$  are suitable for medium temperature range applications, and aluminum, zinc and magnesium for high temperature range applications with a melting temperature ranging from  $400\text{-}700^\circ\text{C}$  [38]. Metallic PCMs generally have high thermal conductivity, in contrast to organic PCMs. However, they have low latent heat combined with high density, resulting in high weight versus thermal storage. For low temperature regimes, metals and metals alloys have latent heats in an order of magnitude lower than similar melting temperature organic PCMs. For higher temperatures, this difference evens out.

## 2.2.3 PCM Selection

There are many possible candidates for PCMs for a given application due to a high number of important properties influencing suitability, but also many restrictions such as melting temperatures and material degradation. Thus, the selection of an ideal PCM is complicated and requires comprehensive knowledge of the PCM application. The following section regarding key indicators for the selection process of an ideal PCM is based on the work of Kristjansson et al. [26].

The analysis presented here is a first order approach only considering conductive heat transfer. Convective effects in PCM materials can be significant for pure PCM systems, but these effects are reduced for an increasing use of heat transfer enhancement (HTE) such as fins or foam. Including the convective effects also increases the complexity of the analysis, thus convective effects are not included as conductive heat transfer is dominant. The first indicator is the energy density of the material, which should be able to store high amounts of energy in limited volumes.

The energy density can be calculated by adding the heat of fusion of the material to the calculated sensible heat capacity from an ambient temperature up to the melting temperature. The volumetric energy density is obtained by multiplying this with the density of the material, equation (2.3).

$$e_v = (c_p \cdot (T_m - T_{amb}) + H_f) \cdot \rho_s \quad (2.3)$$

where  $c_p$  and  $\rho_s$  is the specific heat capacity and solid state density of the PCM material. The heat storage capacity and the supplied heat should be in the same order of magnitude, equation (2.4):

$$e_v \cdot L = \Delta t_{cycle} \cdot \overline{\dot{q}''_{hot}} \quad (2.4)$$

where  $L$  is the heat storage thickness,  $\Delta t_{cycle}$  is the heat cycle duration and  $\overline{\dot{q}''_{hot}}$  is the average heat flux supplied.

The ratio of latent heat to sensible heat storage capacity is another important parameter, equation (2.5). The behavior of the heat storage will be close to a sensible heat storage solution if the latent heat storage capacity is small relative to the sensible heat storage capacity.

$$C_r = \frac{H}{H_f + (c_p \cdot (T_m - T_{amb}))} \quad (2.5)$$

For sensible heat storage the ratio is equal to 0 and 1 for melting temperatures similar to the ambient temperature. This ratio is important in applications where the melting temperature of the PCM varies greatly with the ambient temperature.

Thermal conductivity in PCMs are generally low. To implement a PCM in a heat storage system successfully, a HTE method should be used to both increase the effective thermal conductivity and lower local temperature differences in the heat storage. This can be seen from Fourier's law of heat conduction, equation (2.6)

$$-\frac{dT}{dx} = \frac{\dot{q}''}{k_{eff}} \quad (2.6)$$

where  $k_{eff}$  is the effective conductivity in the PCM, including the effect of the HTE. For the usage of fins as HTE,  $k_{eff}$  is given as:

$$k_{eff} = \varepsilon \cdot k_{PCM} + (1 - \varepsilon) \cdot k_{HTE} \quad (2.7)$$

where  $\varepsilon$  is the volumetric ratio of PCM volume to the total volume.  $k_{PCM}$  and  $k_{HTE}$  is the thermal conductivity's of the PCM material and the HTE system.

To limit temperature gradients in the PCM and to obtain uniform heat release it is important with short distances between the PCM and HTE to reduce thermal resistance from the fin to the PCM. The Biot number, equation (2.8), represents the ratio between the cold side external thermal resistance and the internal conductive thermal resistance.

$$Bi = \frac{h_{cold} \cdot L}{k_{eff}} \quad (2.8)$$

where  $h_{cold}$  is the heat transfer coefficient of the cold side. It is also important to keep the effective thermal conductivity high and the the thickness of the heat storage small to ensure a small Biot number. For a large Biot number,  $Bi \gg 1$ , the temperature difference will be much greater for heat storage hot and cold side than for the cold wall an ambient air. This will result in a LHS heat release similar to that of a sensible heat storage heat release due to temperature gradients caused by a low  $k_{eff}$ .

# 3 — Heating systems for buildings

This chapter will introduce general theory and design of centralized heating systems for buildings and PCM-based heat or cold storage units. There will be an emphasis on heat pumps in centralized heating system as part of the master thesis will focus on heat storage with PCM in combination with a heat pump as a heating system for an office building.

## 3.1 Design of Centralized Heating Systems

Heating systems represent different combinations of equipment used to heat up the interior space of a building. The source of energy powering the system varies and can typically be: Solar, gas, oil, biomass and electricity. Heating systems can be generally divided into two categories:

1. Space heating
2. Central heating

A central heating system generates and distributes heat through a distribution network throughout the building. Often in combination with ventilation heating. The heat is generated in one location typically by using furnaces, boilers or heat pumps. It can also be generated off-site, and delivered through pipes to the central heating system, such as district heating. Furnaces and boilers (non-electric) generate heat through combustion of fuel, often fossil based fuels. The resulting heat is then transferred to air or water/steam and distributed through ducts or pipes to different rooms in the building. The heated air is then mixed with room air through air registers or heat is transferred by the use of radiators or floor piping.

Combustion furnaces and boilers have been widely used for heat generation in residential and commercial buildings traditionally. But as of 2020, Norway prohibits the use of fossil fuels in combustion processes for heating purposes [35]. This is a measure implemented to reduce green house gas emissions. Heat pumps are thus a good alternative to cover the heat demand for a building without relying on fossil fuels, assuming the electricity used to power the heat pumps is produced from renewable sources. It utilizes thermal energy stored in the ambient air, earth or water by moving heat from an outside source to the indoor environment. As heat is being moved, not generated, the heat pump can deliver more thermal energy than it consumes. This reduces the electrical energy required for heating the building, as the heat pump is more energy efficient than an electrical boiler or electrical space heating.

Geothermal heat pumps are often preferred to air source heat pumps in colder climates due to low temperatures and great temperature fluctuations throughout the year. By utilizing the more stable temperatures down in the earth, these fluctuations can be avoided,

which would reduce the heating capacity and efficiency of the heat pump. Geothermal heat pumps requires high initial investment costs dependent on different variables, one being required heating capacity. These heating systems are often dimensioned to cover the baseload, which in practice means to cover the heat demand during normal operating conditions. This is illustrated in Fig. 3.1. To be able to cover the peak load during the coldest days, a backup solution is needed. This can be covered by thermal storage, district heating or an electrical boiler among other solutions.

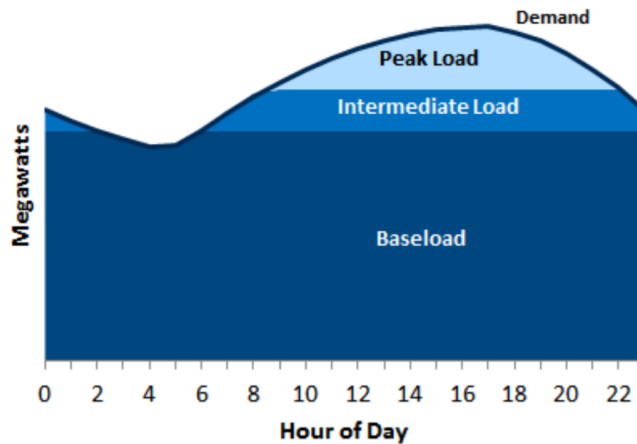


**Figure 3.1:** Illustration of heat demand throughout a day.

To increase the overall efficiency of the heating system different technical solutions can be implemented into the overall system. One solution is waste heat recovery from heat generating processes in the building. For commercial buildings this can be heat generated from a server/inverter room or heat recovery from ventilation exhaust air. Through the use of a heat exchanger, this recovered heat can be used for room/space heating and/or domestic hot water heating. Another solution for increasing the efficiency and thus reducing the need for purchased energy is solar thermal collectors. These are special panels designed to absorb heat which then can be transferred to a fluid. This heat can then be used for domestic hot water and for general heating purposes and will reduce the grid dependency of the building.

## 3.2 Design of PCM-based Heat or Cold Storage Units

### 3.2.1 General

Thermal energy storage can be utilized to reduce peak heating and cooling loads in buildings and to improve the overall performance and reliability of the heating system. The use of TES can help overcome the lack of concurrence between the energy supply and demand which can allow for the exploitation of solar energy and waste heat [12]. PCMs provide a compact and efficient alternative for short-term thermal energy storage, however



are limited by their low thermal conductivities. This can be compensated for by an effective design of the PCM TES system (LHS system). Section 3.2 focuses on presenting research on the design of PCM-based heat or cold storage units for thermal energy systems based on relevant literature.

There are several ways to incorporate PCM technology for heat storage purposes in building environments. PCMs can be included in building components for passive heating and cooling encapsulated in concrete, gypsum boards, ceilings and floors [6]. Passive thermal energy storage systems can effectively improve the utilization of the naturally available heat energy sources to maintain the desired comfort conditions in a building whilst reducing the use of mechanically driven heating or cooling systems.

The use of active TES systems ensures for a high degree of control over the indoor environmental conditions and improves the method of storing heat energy [38]. The goal of these systems is to provide free cooling or to shift the thermal load in HVAC systems or domestic hot water applications. The integration of TES systems in a building can be done using the external parts of the building (floors, walls, facades and ceiling), in the ventilation system, PV systems and in storage tanks. Fig. 3.2 illustrates different solutions for integration of TES in a building. The focus for this work will be on TES systems containing a PCM-based heat/cold storage tank/unit referred to as a LHS system from here on. Other active and passive TES solutions will not be discussed further.

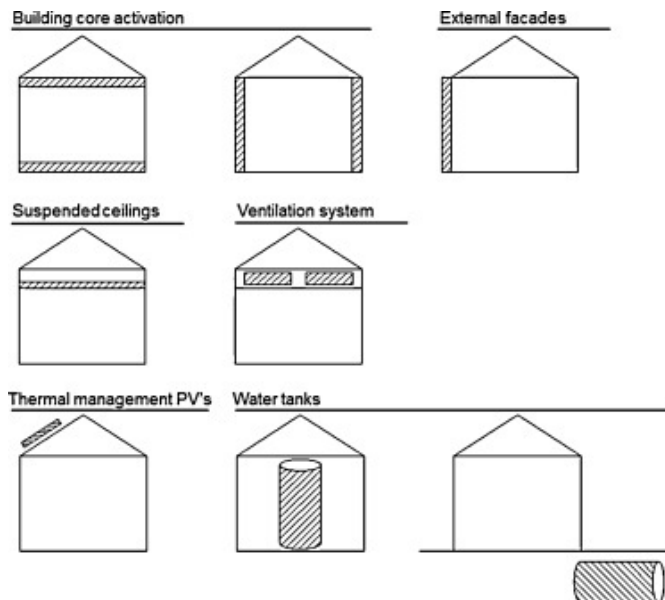


**Figure 3.2:** Different ways of integrating TES systems in a building [38].

The main components of a PCM-based heat or cold storage unit are:

- Storage tank
- Storage medium - PCM
- Heat transfer fluid (HTF)
- Distribution system
- Sensors and control system

The storage tank holds the PCM material and the heat transfer fluid, typically water or air, which transfers heat/cold between the HTF and PCM during charging or discharging cycles. The distribution system transports the heat from the LHS system through pipes/ducts by the use of pumps/fans. Sensors and control strategies are required in the TES system to appropriately control the charging/discharging cycles to match the building energy demand.

The interest on PCM-based heat or cold storage has increased greatly the past years. The number of published articles on the topic proves that a lot of research is being done on the field, seen in Fig. 3.3

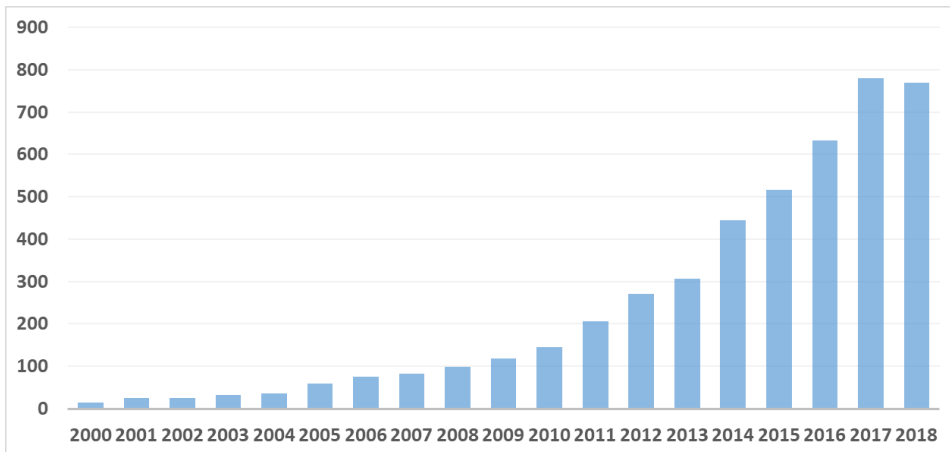


**Figure 3.3:** Number of published articles on the topic "PCM heat storage" since 2000. Source: Web of Science.

### 3.2.2 Design Criteria

Pavlov and Olesen [31] describes the following criteria and steps for design and evaluation of TES systems: First, it is required to determine the energy load profile for the building. Variables having an impact on this are listed as use of the building, internal heat loads, and local climatic conditions. It is then necessary to determine the type and amount of thermal storage required for the specific application, the effect of the storage on overall system performance, cost and reliability, and the technology/design available for TES. It is important to characterize the TES system based on the storage duration required. This can

be blatantly divided into short-term and long-term storage. Short-term storage describes peak loads ranging from hours to a day with the goal to reduce system size and take advantage of daily structure of energy tariffs. Long-term storage denotes storage related to waste heat or seasonal energy loads, often with a delay of some weeks to several months. Regarding the appropriate amount of storage needed, improvement is needed for the current TES sizing techniques. Completed projects have shown a tendency for both over- and undersizing which can result in a high initial cost, waste of energy or a poor indoor environment. It is thus paramount to evaluate the effect of the TES on the overall energy system performance in details, to obtain an economic justification for a TES system.

### 3.2.3 PCM Containers and Encapsulation

There are a range of commercially available PCMs from different suppliers. Tab. 3.1 lists PCMs with their thermal properties for a melting temperature ranging from 29 to 37°C.

**Table 3.1:** Selection of commercially available PCMs.

Product	Type	Melting point [°C]	Heat of fusion [ $\frac{kJ}{kg}$ ]	Thermal conductivity [ $\frac{W}{m \cdot K}$ ]	Manufacturer
L29T	Salt hydrate	29	188	1	TEAP
HS29P	Salt hydrate	29	190	0.54	RGEES
S30	Salt hydrate	30	190	0.48	PCM Products
SP31	Salt hydrate	31	210	0.6	Rubitherm GmbH
OM32P	Organic	32	235	n/a	RGEES
HD32	Salt hydrate	32	150	n/a	Salca BV
C32	Inorganic	32	162	0.6	PCM Products
S32	Salt hydrate	32	200	0.51	PCM Products
A32	Organic	32	130	0.21	PCM Products
E32	Eutectic	32	243	0.56	Pcm Products
PCM32	Organic	32	185	n/a	Microtek
E34	Eutectic	34	240	0.54	PCM Products
A36	Organic	36	217	0.18	PCM Products
L36S	Salt hydrate	36	260	0.6	TEAP
E37	Eutectic	37	213	0.54	PCM Products
A37	Organic	36	235	0.18	PCM Products
CT37	Organic	37	202	0.24	CrodaTherm
PCM37	Organic	37	215	n/a	Microtek

The encapsulation method is fundamental to PCM application. Manufacturers of PCM utilize different methods. PCM Products has developed macro-encapsulation solutions and has patented its own HDPE capsules as well as offering raw PCM material [32]. Rubitherm offers macro-encapsulated PCM based on plastic or metallic containers for bulk storage [36]. PCM encapsulation methods and technologies are being continually refined to in-

crease performance. For active systems the most common solution for LHS is bulk storage or macro-encapsulation. For bulk storage, PCM is enclosed in large tanks. This is a cost effective method due to its simplicity. However, challenges are experienced with low thermal conductivity generating fluctuating performance [7]. HTE methods have been investigated by agitation or by increasing the heat transfer surface area [2]. Macro-encapsulation is the inclusion of PCM in some sort of a container. This is typically tubes, pouches, spheres, panels or other building parts. They can be used directly as heat exchangers or be integrated in building products. Macro-encapsulation containers are generally larger than 1 cm in diameter. In addition to holding the PCM, the container isolates the PCM from chemical interaction with other components and exposure to the environment. It also improves handling of PCM and reduces external volume changes [6].

To ensure thermal performance for a bulk storage PCM system, there must be a correspondence between the size and shape of the PCM container and the melting/solidification time of the PCM and the daily heat demand. Thin heat pipes, cylindrical containers, or rectangular containers are typically used for the containment of PCM. A survey based on previously published papers on latent heat TES reveals that rectangular and cylindrical containers are most often selected for PCM containers [3]. The same survey concludes that the shell and tube system is most analyzed. Figure 3.4 shows illustrations of cylindrical and shell and tube containers.

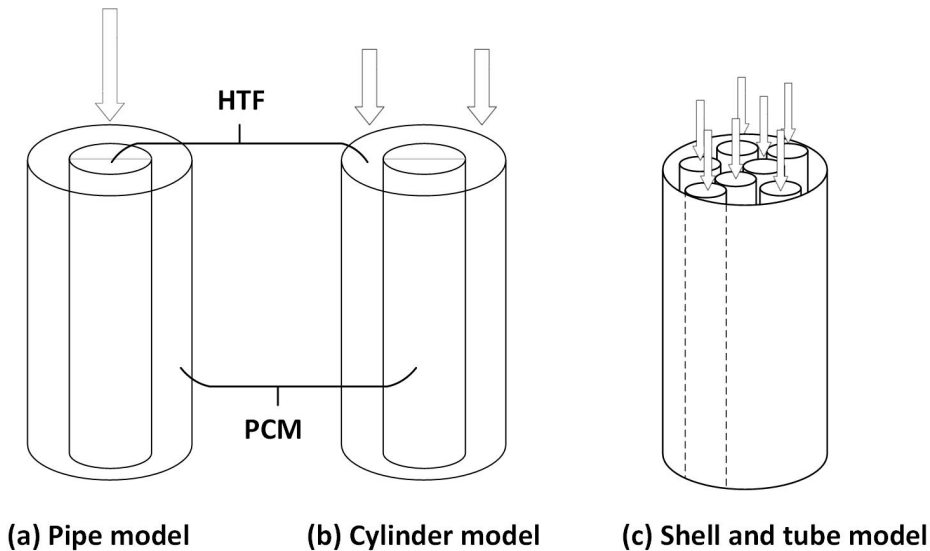


**Figure 3.4:** Classification of PCM containers.

### 3.2.3.1 Cylindrical PCM Container Configuration

Cylindrical PCM containers can be distinguished by three different setups [3]. The first, illustrated in Fig. 3.4a, the heat transfer fluid flows through a centered tube. PCM occupies the surround shell. The second configuration consists of HTF flowing in the shell, while

PCM occupies the centered tube, seen in Fig. 3.4b. Esen et al. [16] compared the two setups theoretically by studying and comparing impacts of different thermal and geometrical properties such as cylinder radius, PCM volume, inlet temperatures and mass flow rates of the HTF. The results showed a shorter melting time for the pipe model because the melting time increases with thickness of the PCM. Agyenim et al. [3] adds that the pipe model also will have a lower rate of heat loss to the environment due to heat supplied by the HTF in the center will end up heating the PCM. The third cylindrical PCM container setup is the shell and tube, which is normally used to increase heat transfer in the PCM system. Agyenim et al. [1] compared heat storage and heat transfer in a single tube and a multitube horizontal shell and tube system experimentally. It was found that the effect of several convective heat transfer dominated the heat transfer for the shell and tube compared to conductive heat transfer for the pipe model (single tube). Temperature gradients determined in the axial directions were for the pipe model and the shell and tube setup was found to represent respectively 2.5% and 3.5% of the temperature gradients in the radial direction, showing two-dimensional heat transfer for both cylindrical configurations. As a result of natural convection, the shape of the solid-liquid interface fluid flow was greatly altered in the shell and tube, resulting in a complete melting time of 5 h compared to 8 h for the pipe model. The shell and tube system was thus recommended for charging of PCMs.

### 3.2.3.2 Cylindrical PCM Container Flow Directions

For a cylindrical PCM container there are two different configurations for the HTF flow direction. The flow can be introduced from the same end during both charging and discharging (parallel flow) or the flow can be introduced from opposite sides during charging and discharging (co-current flow). Fig. 3.5 illustrates the different configurations. Gong and Mujumdar [18] studied the effect of parallel and co-current flow configurations through numerical simulations. The results showed a 5 % increase in energy charge/discharge rate for parallel flow. This increase was a product of a higher temperature difference at the inlet during parallel flow that led to a larger penetration depth for the solid-liquid interface in the PCM. In addition, co-current flow showed significant supercooling in the inlet region for the charge/discharge process.

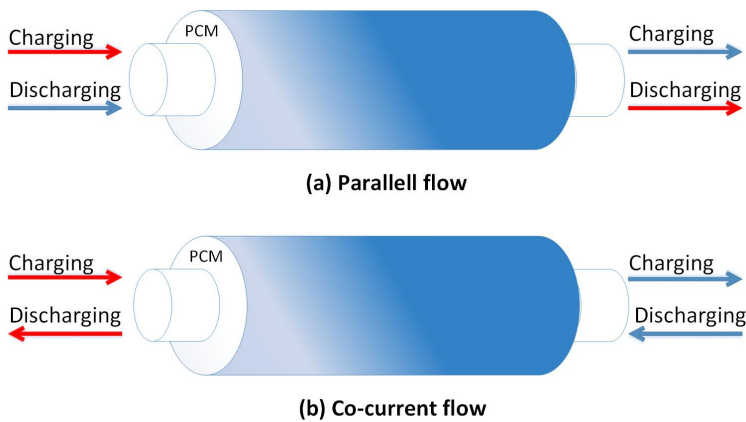


**Figure 3.5:** Illustration of parallel and co-current flow in a shell and tube system.

### 3.2.4 Heat Transfer Enhancement

The heat transfer rate is determined by thermal conductivity, heat exchange area, temperature difference between the HTF and the PCM and the operation of the LHS system. Due to the low thermal conductivity of PCMs, enhancement of heat transfer is critical for bulk storage and encapsulated PCM. There are several methods to do this, and various solutions has been proposed by researchers. Including bubble agitation, finned tubes, metal matrix insertion, PCM mixed with high conductive particles, shell and tube and micro-encapsulation to list some. Fig. 3.6 shows different fin geometry for tubes.

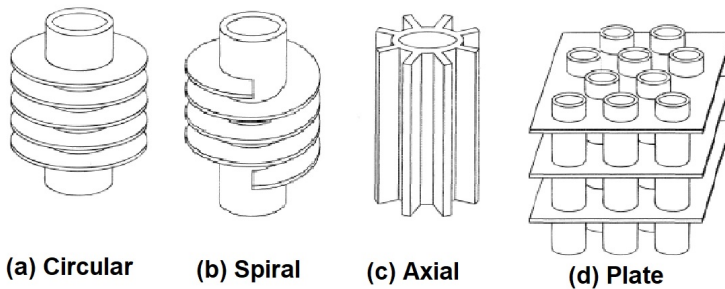


**Figure 3.6:** Different fin geometry for increased HTE in tubes.

Rahimi et al. [34] showed how the melting and solidification time for a LHS system is reduced when introducing plate fins and changing the number of fins in a fin and tube experimental setup. Figure 3.7 shows how both solidification and melting time of PCM is greatly reduced when adding fins.  $F_p$  in the figure denotes the fin pitch for the experimental

setup. Rahimi et al. [34] argues that the solidification time is influenced greater due to conduction being the dominant heat transfer mechanism during solidification.

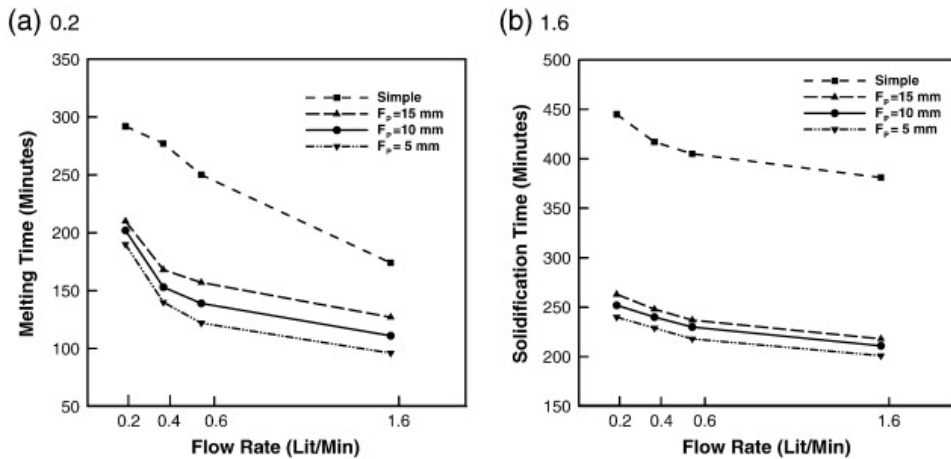


**Figure 3.7:** Melting time (a) and solidification time (b) for different mass flow rates and fin pitches [34].

Choi and Kim [9] examined experimentally heat transfer in a circular finned and un-finned latent heat storage system using  $\text{MgCl}_2 \cdot 6\text{H}_2\text{O}$  as PCM. The study showed a uniformly larger temperature gradient in the radial direction for the finned tube system. The heat transfer coefficient was reportedly 3.5 times larger for the finned tube system inside the finned section, and gradually decreased away from the fin. Thermal performance was found to be more dependent on inlet temperature than by mass flow rate of HTF (air) in the unfinned tube system. The effect of the HTF mass flow rate on the thermal performance is more noticeable for the finned tube system. Fig. 3.8 shows the heat transfer coefficient plotted against PCM crystal volume for the finned and unfinned tube at different inlet temperatures.

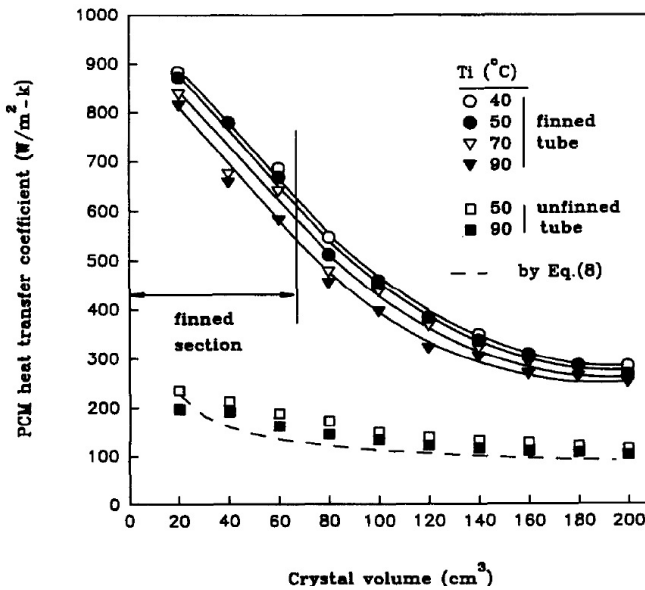


**Figure 3.8:** Heat transfer coefficient between HTF and PCM for different inlet temperatures [9].

A mathematical model was developed by Horbaniuc et al. [21] to predict the position of the solid-liquid interface at a given time for PCM surrounding a heated tube with axial fins. By superimposing the angular and radial solid layer on the fin surface around the cylindrical tube wall, complete solidification time could be determined as a function of the total number of fins. The number of fins needed for a predetermined solidification time can also be derived from this model. Velraj et al. [43] experimentally investigated heat transfer enhancement in a latent heat storage system, consisting of paraffin PCM in a vertically orientated aluminum storage tube surrounded by a water filled outer cylinder. Three different HTE techniques were tested; fins, lessing rings and bubble agitation, illustrated in Fig. 3.9.



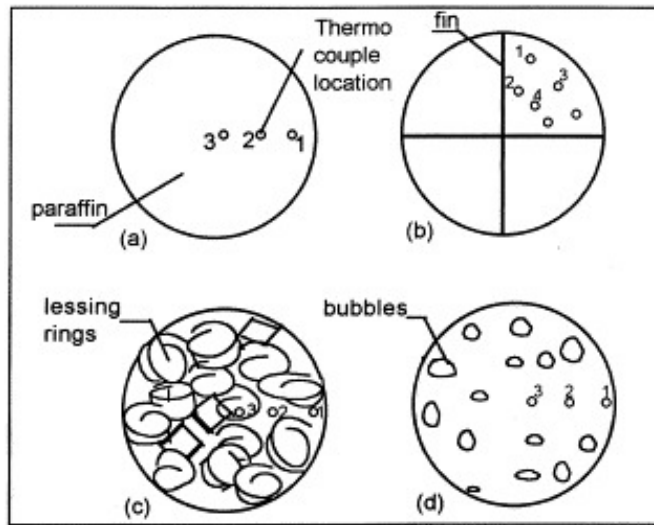


**Figure 3.9:** Heat transfer enhancement methods [43].

The results from bubble agitation were not presented, as there was recorded no significant augmentation effect during solidification. Heat transfer during melting was reported to increase to some extent due to natural convection induced by the movement of bubbles. Both fins and lessing rings results showed increased heat transfer rates by reduced solidification time of the PCM. For the lesser rings, the effective thermal conductivity,  $k_e$ , was calculated to be  $2 \frac{W}{m^2K}$ . This is ten times greater than the thermal conductivity of paraffin. This HTE reduced the PCM volume by 20%. Fig. 3.10 shows the time required for complete solidification of the paraffin PCM surrounded by water at a constant temperature for plain PCM in a tube and for the two different HTE methods. The reduction in total heat extracted for the HTE methods is due to the volume occupied by the HTE material.

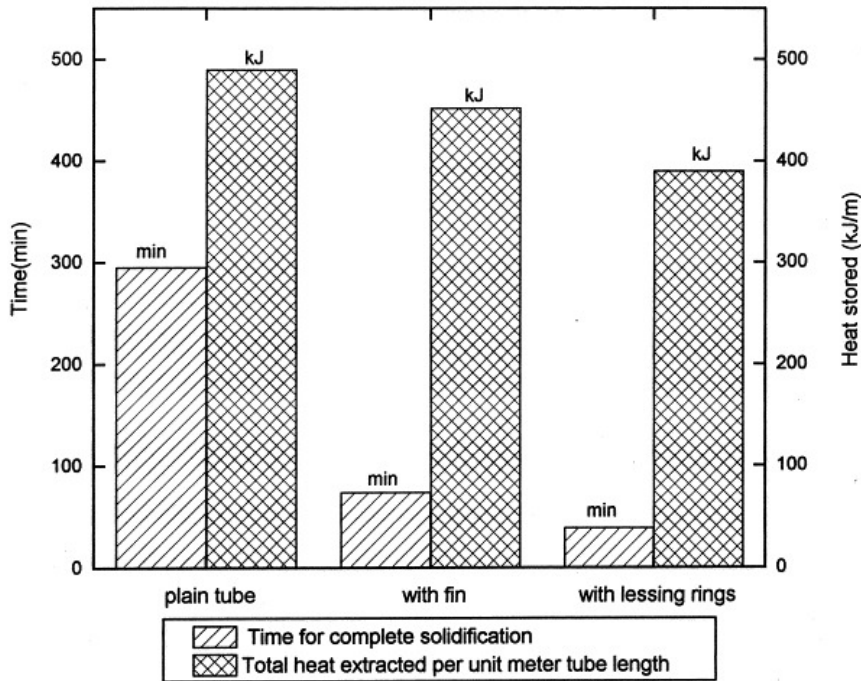


Figure 3.10: Solidification time for different HTE methods [43].

Hamada et al. [19] compared the effects of adding heat transfer enhancing particles to the PCM on the overall heat transfer rates. This was done by adding carbon-fiber chips and carbon brushes with different thermal properties. Both methods proved effective in improving the heat transfer in the PCM. The carbon-fiber chips showed the highest effective thermal conductivity of the bulk. However, the carbon-fiber chips reportedly had a higher thermal resistance near the heat transfer surface, resulting in a higher overall heat transfer coefficient for the carbon brushes. As a consequence, the authors conclude that the carbon brushes are superior to the carbon-fiber chips under the current experimental conditions.

### 3.2.5 LHS Integration with Heat Pump

Comprehensive work has been done to increase the heat transfer rates within LHS systems by utilizing heat transfer enhancement techniques in numerical investigations and in experimental setups. However, only a few full-scale active LHS systems are in operation, making it challenging to document the potential upsides of coupling a LHS system to a heat pump for peak shaving and heating purposes. Hirmiz et al. [20] studied the integration of LHS systems into heat pump systems to improve the demand side flexibility and, ideally, the strategy for the LHS system to cover the complete heat demand during peak periods. By utilizing a TRNSYS numerical model, it was concluded that a LHS system can completely offset peak heat demand periods within 2 to 6 hours, reducing peaks in the power grid. Through modeling and measurement data analysis, Jokiel et al. [23] eval-

uated a LHS system installed to reduce the required chiller capacity for three ammonia chillers/heat pumps covering the base load for heating/cooling at the Bergen University College (Norway). A dynamic system model was developed using Modelica [28] to better understand the dynamics of melting and solidification of the PCM. The model proved to correctly predict the measured data, within an acceptable accuracy, especially regarding the accumulated values of absorbed and released heat. Bonamente et al. [4] studied the potential for system optimization in an existing ground-source heat pump heating system by implementing a TES unit. Computational fluid dynamic calculations were carried out and validated against measured data using two TES solutions: one using water as storage medium, and the other using PCM. Results showed that the COP of the system was increased from 2.9 to 3.2 and 3.4 for, respectively, heating and cooling modes when using water as TES medium. By using a PCM, the system COP was increased to 4.13 and 5.89 for, respectively, heating and cooling modes. In addition, the total volume of the PCM thermal storage was 10 times more compact compared to the water tank system making it more suitable for indoor installation and use. Shifting the cooling load during simulated summer conditions was experimentally tested by Moreno et al. [29], by coupling a TES system to a heat pump. Thermal behaviour for the TES system was evaluated for cold storage and for space cooling. Two different TES configurations were tested, one using water and the other using PCM. The latter configuration utilized macro-encapsulated PCM with a phase change temperature of 10 C. It was concluded that PCM storage is favourable to water storage. With identical volumes, the PCM tank was able to store 35.5 % more cold energy on average compared to the water storage tank. Other results indicated that by increasing the heat transfer rate for the PCM storage, it could store 14.5 % more cold energy, while delivering an acceptable indoor temperature for a 20.65 % longer duration compared to the water storage. Zhang et al. [45] constructed a simplified model to study the impact of LH TES location in a buildings cooling and heating system. It was deduced that ultimately, the optimal TES location in a heating system is highly dependent on user characteristics and the thermal performance of the heating equipment. However, results showed that only downstream TES can reduce the installed capacity of a heat pump.

# 4 — Case Study: ZEB Flexible Laboratory

## 4.1 General

This chapter aims to propose a heat storage design for a ZEB building to be built in Trondheim in the fall of 2019. Fig. 4.1 shows an illustration of the proposed design. The building will be the product of a cooperation project between NTNU and SINTEF with the goal to be a ZEB-COM office building functioning partly as a living laboratory to test new technologies and operation strategies. In order to achieve the ZEB-COM standard, the energy use and greenhouse gas emission from materials must be reduced sufficiently. In addition, the building must produce renewable energy to the extent that it compensates for all the greenhouse gas emissions involved with the materials and the construction of the building [22]. A PCM thermal energy storage system will be a part of a hydronic heating system and positioned in the water distribution loop. Heat will be utilized from two additional sources: exhaust ventilation air and waste heat from an inverter-room. Two liquid-liquid heat pumps are dimensioned to cover 50% of the peak power and up to 100% of the heat demand combined with the heat storage unit. Local district heating will be available as backup to cover the peak power demand for the coldest days. The heat demand for the building is calculated through simulations in IDA ICE and will be used as a basis for the dimensioning of the heat storage unit.

The goal with installing the PCM TES technology is to obtain the following:

- Balance energy demand and supply on a daily and weekly basis
- Reduce peak power demand
- Reduce economical costs
- Reduce CO<sub>2</sub>-emissions
- Increase system efficiency



Figure 4.1: ZEB Flexible Laboratory [22].

## 4.2 Latent Heat Storage Unit

Two liquid-liquid heat pumps will be the heat source for the buildings hydronic heating system. The dimensioning temperatures are a water supply temperature of  $40^{\circ}\text{C}$  and a return temperature of  $30^{\circ}\text{C}$ . This heating system, combined with the TES and various heat sources, will have a calculated SCOP of 5. Fig. 4.2 shows the system diagram for the hydronic heating system for the ZEB Flex Laboratory building with the LHS system outlined in blue. The red line shows the hydronic main flow line with the LHS system connected upstream of the heat pump (green). All other connections (yellow) are different heat sinks and heat sources from e.g solar, inverter room and exhaust ventilation air. Throughout the heating circuit, preheating of domestic hot water, room radiators and heat exchangers providing heated air for ventilation are used as heat sinks to heat up the building. Additional components enabling research experiments in the different rooms of the buildings are also planned but constitute minor heat sinks and heat sources on the heating circuit and thus are out of the scope of the present study. Without the LHS unit, the heat pump is meant to cover the maximum heat demand of the building, calculated to ca. 26 kW, necessary to maintain all rooms in the building at a comfortable temperature on the coldest days of the year in Trondheim (Norway). Using the LHS unit to support peak heating demands, the

size and nominal effect of the heat pump can be significantly reduced, so that it operates more effectively.

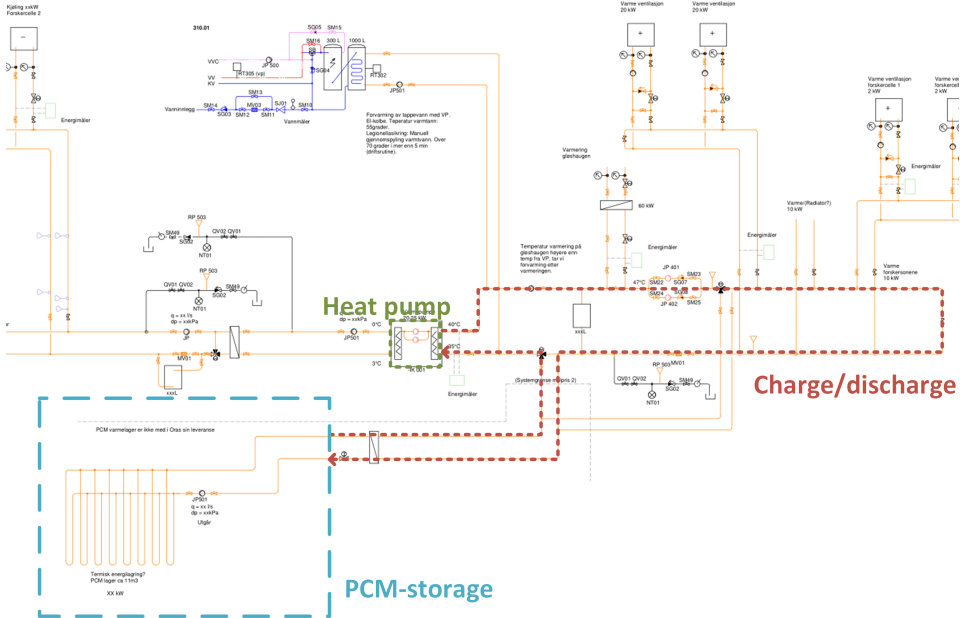
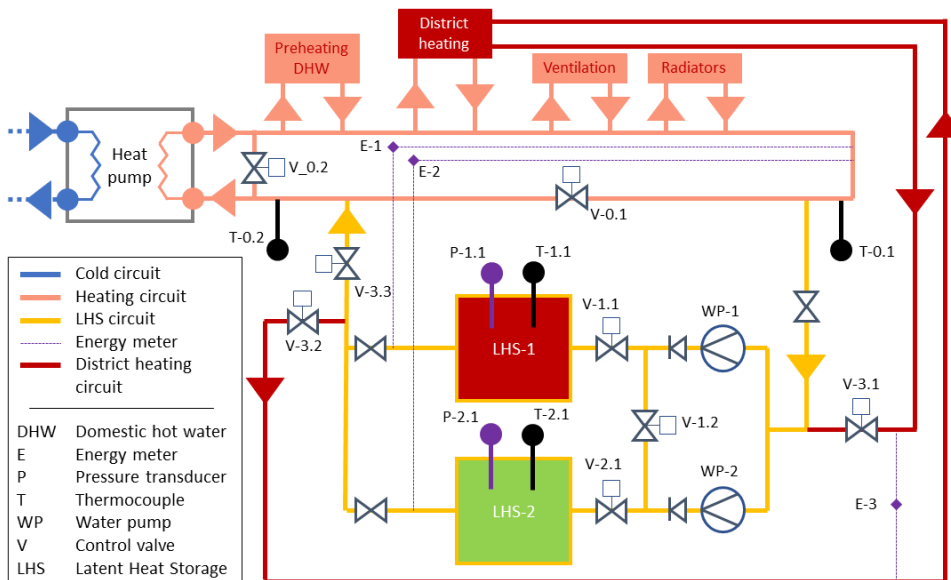


Figure 4.2: Hydronic heating system diagram for ZEB Flex Laboratory.

### 4.2.1 Unit Integration

Among the possible scenarios to integrate the LHS unit in the centralized heating system, the integration enabling thermal buffering to support the heat pump was selected. Fig. 4.3 shows this configuration. Depending on the heating demand in the building, the return temperature of the heating loop might be lower than  $34^{\circ}\text{C}$ , and thus require additional power from the heat pump to continually obtaining  $40^{\circ}\text{C}$  as outlet temperature. Integrating the LHS unit downstream from the heat pump, as discussed in Section 3.2.5, with the option to circulate the return water through it or not, provides the opportunity to both charge and discharge the LHS unit, while levelling out the power demand of the heat pump. Charging the LHS unit occurs when the heating demand is low, using  $40^{\circ}\text{C}$  as inlet temperature, as it is generated by the heat pump. Using a PCM with phase change temperature within  $34\text{--}37^{\circ}\text{C}$ , return water at lower temperature than  $34^{\circ}\text{C}$  can circulate through the charged LHS unit and be heated up before entering the heat pump. Additionally, the LHS unit can be directly charged using the district heating loop providing hot water at  $45^{\circ}\text{C}$ . In Fig. 4.3 two LHS units (LHS-1 and LHS-2) are integrated in the heating system, to ultimately allow for research experiments using various heat exchanger designs and test the thermal performance of several PCM. The present study focuses only on the design of LHS-1.



**Figure 4.3:** Process diagram of the centralized heating system illustrating the LHS units.

Another feature available with this integration is the opportunity to use the LHS unit as a direct heat source in the building heating loop. This is meant to occur when the LHS unit is charged and the heating demand in the building is relatively low. Therefore, the heat pump can be bypassed, reducing significantly the energy use during these low-demand periods. This operational mode is especially interesting if energy price is integrated in the control system of the overall heating system.

## 4.2.2 Control Strategy

As shown in Fig. 4.3, the system allows for a variety of control strategies through a large number of control valves and two regulated water pumps. Two strategies are selected:

- A temperature-controlled strategy for charging and discharging using only the heat pump as heat source and heat sink
- A price-controlled strategy where the energy price is taken into account to decide when to use district heating for LHS charging and when to use the LHS unit as direct heat sources for the building heating circuit.

In both cases, the energy level of the LHS units is followed up using thermocouples located at various locations in the unit. Full charge is indicated by an average PCM temperature 4 K above its melting temperature range. Full discharge is indicated by an average PCM temperature 4 K below its solidification temperature range. In addition, three energy meters will enable to track the effect and accumulated transferred energy to follow up the thermal performance of the two units. The control system of the LHS system is to be fully integrated in the building control system, which will include a "researcher mode" to allow

customizing and testing various control strategies. The temperature-controlled strategy is illustrated in Fig. 4.4.

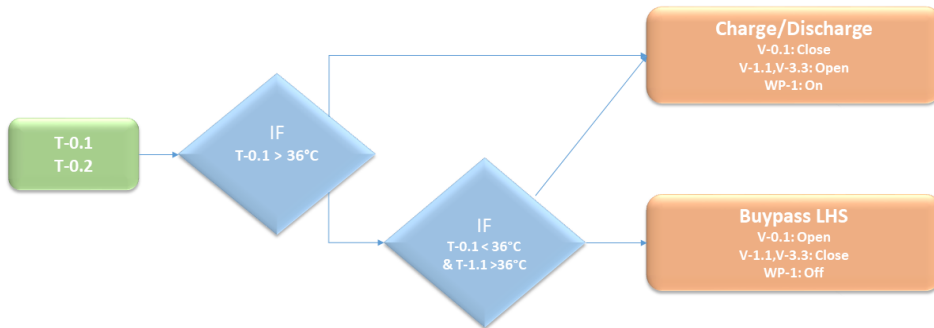


**Figure 4.4:** Control strategy for LHS-1.

### 4.2.3 PCM Selection

The most suitable PCM for the LHS unit should primarily have a melting temperature within 34-37°C, which yields only a limited range of commercially available PCMs. Tab. 4.1 lists a selection of commercial PCMs with melting temperatures ranging from 34°C to 37°C, as well as some of their thermodynamic properties given by the manufacturers.

**Table 4.1:** Commercial PCMs qualified for the LHS unit.

Product	Type	Melting point [°C]	Heat of fusion [ $\frac{kJ}{kg}$ ]	Thermal conductivity [ $\frac{W}{m \cdot K}$ ]	Manufacturer
E34	Eutectic	34	240	0.54	PCM Products
A36	Organic	36	217	0.18	PCM Products
L36S	Salt hydrate	36	260	0.6	TEAP
E37	Eutectic	37	213	0.54	PCM Products
A37	Organic	36	235	0.18	PCM Products
CT37	Organic	37	202	0.24	Croda
PCM37	Organic	37	215	n/a	Microtek

After investigation of the pre-selected commercial PCMs listed in Table 1 for the melting temperature range 34-37°C, the PCM CrodaTherm 37 (CT37) was selected. CT37 is a water-insoluble organic PCM, derived from plant-based feedstocks [10]. The PCM appears as a crystalline wax in solid state and oily liquid above melting temperature. The main arguments in favour of this PCM are its low degree of supercooling (cf. Tab. 4.2), its low-carbon footprint as well as its affordable cost. In addition, CT37 has low flammability, which is an essential criterion in buildings. A sample of CT37 received by CrodaTherm was analysed by TGA/DSC at the SINTEF Energy Laboratory to evaluate the thermodynamic performance of the PCM. A measurement of 10 melting/solidification cycles was



performed using a Digital Scanning Calorimetry (DSC) device, with controlled heating and cooling rates of 1 K/min ranging from 30°C to 50°C, in a nitrogen atmosphere. The results are shown in Fig. 4.5. As indicated by the manufacturer, the first melting displays a significantly larger latent heat of fusion than the following melting/solidification cycles. Taking into account only the 9 following cycles, CT37 remains absolutely stable, yielding very similar heat flow patterns. The average latent heat of fusion is 198.6 kJ/kg (+/- 0.9 %) and the average latent heat of crystallisation is 196.4 kJ/kg (+/- 0.7 %). The average peak melting temperature peak is 36.5°C (+/- 0.3 %) and the average solidification temperature peak is 34.5°C (+/- 0.1 %). The weight loss is measured to 0.04 % along the first two cycles and then remains stable for the following 8 cycles. Note that thermodynamic property measurements might be variable from one device to another and is also known to depend on the sample mass and measurement procedure.

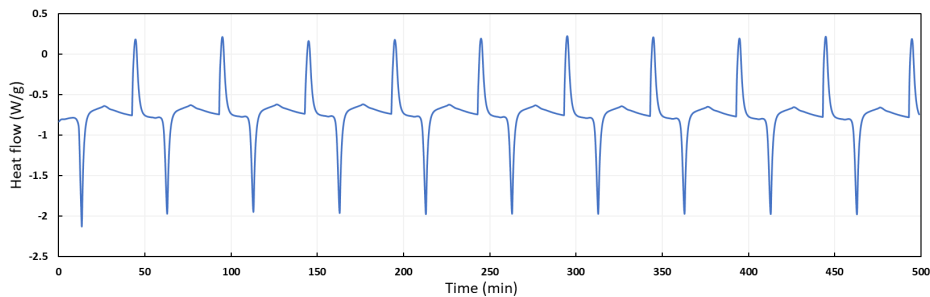


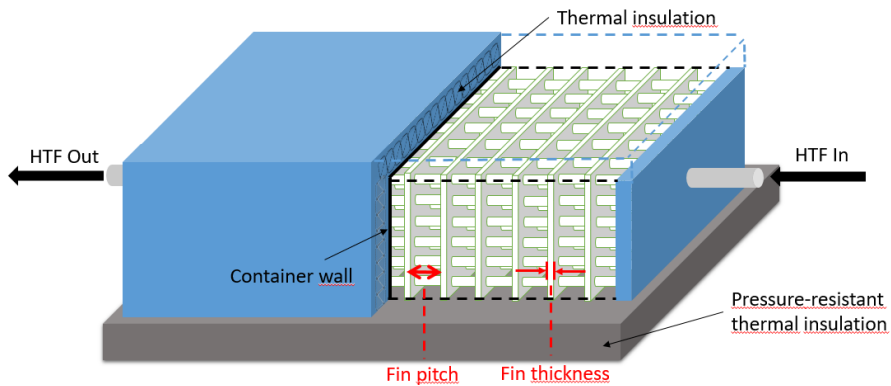
**Figure 4.5:** Heat flow absorbed and released by a sample of CT37 for 10 melting/solidification cycles measured with DSC.

## 4.2.4 Unit Design

The general design parameter of LHS-1 are given in Table 4.2. The LHS unit dimensions are the first constraints to consider for the unit design due to the architecture of the building, limiting the access into the technical room through a 1.8-m wide corridor. This justifies the idea of having two LHS units whose dimensions allow to enter the building (see Table 4.2). The design of LHS-1, shown in Fig. 4.3, is based on a plate fin-and-tube heat exchanger, filled with PCM. The design maximizes the amount of PCM that can be stored with regards to the limiting physical dimensions of accessing the building. Plate fins are used to increase the heat transfer between the HTF piping and the PCM. Water from the heating circuit circulates in the tubes. The design parameters of the fin and tube heat exchanger are discussed in Section 5. Headers at both ends of the unit enable a homogeneous distribution of the water across the tubes. A thick thermal insulation around the LHS-unit allows for a theoretical heat loss under 2 % per 24 h. Fig. 4.6 shows the theoretical heat loss through the container walls for different insulation thicknesses.

**Table 4.2:** General design parameters of LHS-1.

Properties	Unit	Value
Dimensions of unit (height × width × length)	[m]	1.5 × 1.4 × 2.5
Measured PCM melting temperature range and peak	[°C]	35-39 (36.5)
Measured PCM solidification temperature range and peak	[°C]	33-35.5 (34.5)
Measured PCM latent heat of fusion	[ $\frac{kJ}{kg}$ ]	198.6
Measured PCM latent heat of crystallisation	[ $\frac{kJ}{kg}$ ]	196.4
PCM density	[ $\frac{kg}{m^3}$ ]	957 (s), 819 (l)
PCM thermal conductivity	[ $\frac{W}{m \cdot K}$ ]	0.24
PCM specific heat capacity	[ $\frac{kJ}{kg \cdot K}$ ]	2.3 (s), 1.4 (l)
PCM degradation temperature	[°C]	50
Theoretical thermal storage capacity	[kWh]	325
PCM degradation temperature	[°C]	90 %

**Figure 4.6:** Illustration of LHS unit.

To design and dimension a well-functional storage system, it is crucial with knowledge about the buildings heat demand and about the dynamic behaviour of the LHS system during charging and discharging cycles. Numerical simulations can provide new information about LHS system performance, and thus, dynamic modeling of the thermal storage is discussed further in Chapter 5.

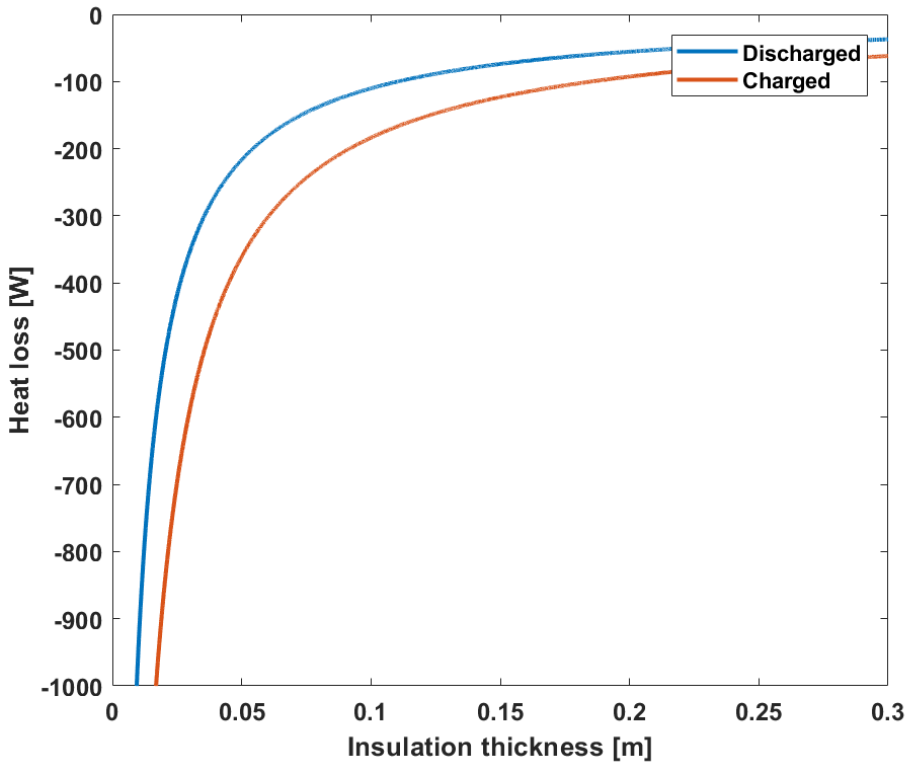


**Figure 4.7:** Heat loss through LHS unit container wall for different insulation thickness. Assuming no loss through radiation. See Appendix E for thermal properties of tank components.

## 4.2.5 HTF Distribution and Pump Power

There are a range of possible ways to circulate the HTF (water) through the LHS unit for a specific amount of tubes going through the unit. As the HTF enters the header it can move through the unit as one flow doing multiple passes by using bends, connecting different tubes in the unit. For this pipe configuration, the mass flow in the HTF tubes is equal to the HTF inlet mass flow. Or the inlet header flow can be divided into several individual separate flows (SF) that will travel through the LHS unit at reduced mass flow relative to the number of SF. Fig. 4.8 illustrates these different designs for a configuration of 16 tubes. The case with one separate HTF flow yields the highest heat transfer rates, due to the tube-side heat transfer coefficient being a product of the Reynolds number of the flow. Because the higher mass flow for this configuration, the pressure drop will also be largest for this case.

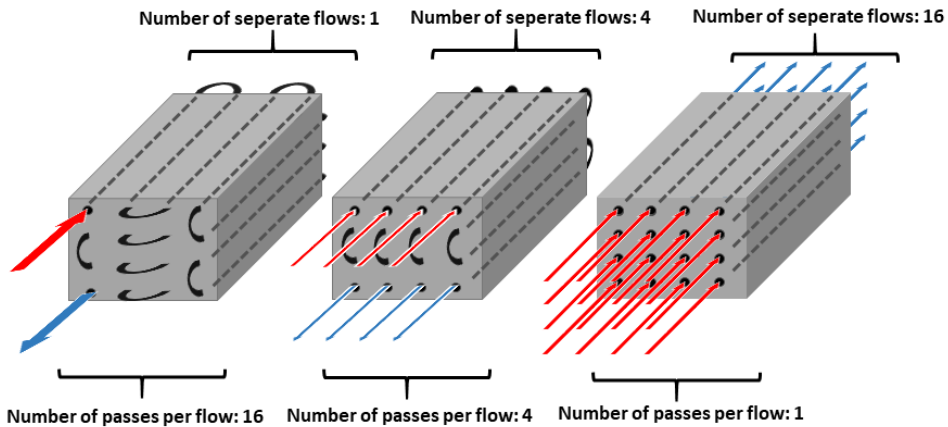


**Figure 4.8:** Illustration of different pipe flow configurations for the LHS unit.

Based on results presented and discussed in Section 6.4, the pump power requirements to compensate for pressure drop through the LHS unit (entrance header, HTF tubes and exit header) is calculated for different HTF pipe configurations. The power requirement is calculated using a safety factor of two times the pressure drop and assuming an overall pump efficiency of 70 %. The resulting required pump power is listed in Tab. 4.3.

**Table 4.3:** Required pump power for different LHS pipe configurations

Pipe configuration - Number of separate flows	Pump power [kW]
5	44.6
15	3.2
45	0.3
75	0.095

#### 4.2.6 Other Considerations

Legionella contamination from the LHS unit should not pose a potential problem, as the unit is integrated in a closed loop hydronic system. However, the ideal growth conditions for the legionella bacteria (37°C) [13], matches the thermal conditions of the unit. To avoid contact with legionella aerosols, the drainage pipe of the HTF should be placed far down in the drain.

### 4.3 Building Heat Demand

During the winter the LHS system will be charged by the heat pumps when the heat demand is low, typically during the night when the building is empty. It is critical that during this phase, the return temperature of the water is greater than the melting temperature of the PCM to invoke latent heat storage. During peak heat demand the PCM TES will be

discharged to increase the return temperature of the water in the hydronic system. During periods with low heat demand or when the LHS system is already discharged during a period with large heat demand, the LHS system will be bypassed and in standby mode. The buildings heat demand over a year has been calculated externally in the simulation tool IDA ICE [27]. Fig. 4.9 and Fig. 4.10 shows a 1-week and 3-week period during January when the heat demand is highest considering the heat demand throughout a whole year. The dotted constant line represents the value where the area over and under this line equals to zero. In other words, that there is an energy balance between charging and discharging the LHS system, assuming there is no heat loss in the LHS system, This line equals to 16.2 kW and 13.27 kW for respectively the 1-week and 3-week heat demand period. With a heat pump delivering these heat output rates, the LHS system shall in theory be able to assist the heat pump in delivering sufficient amounts of heat during peak heat demand. Assuming the LHS system is fully charged prior to a discharge period.

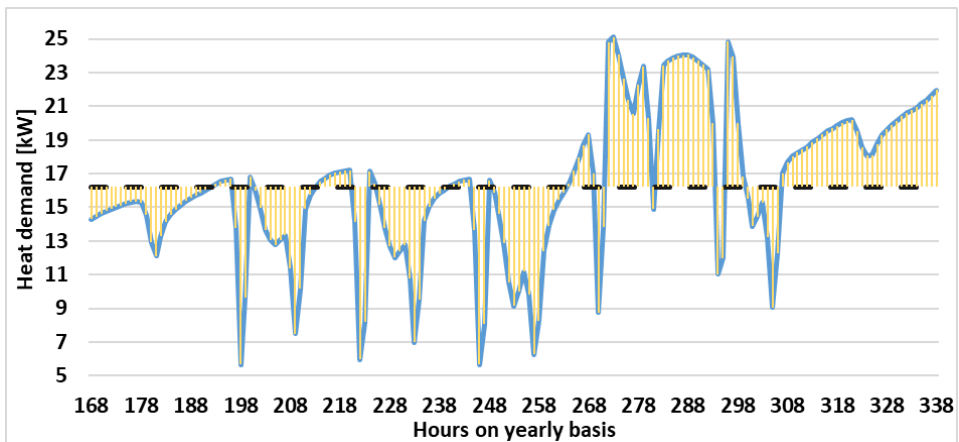


**Figure 4.9:** Heat demand for the coldest week in January.

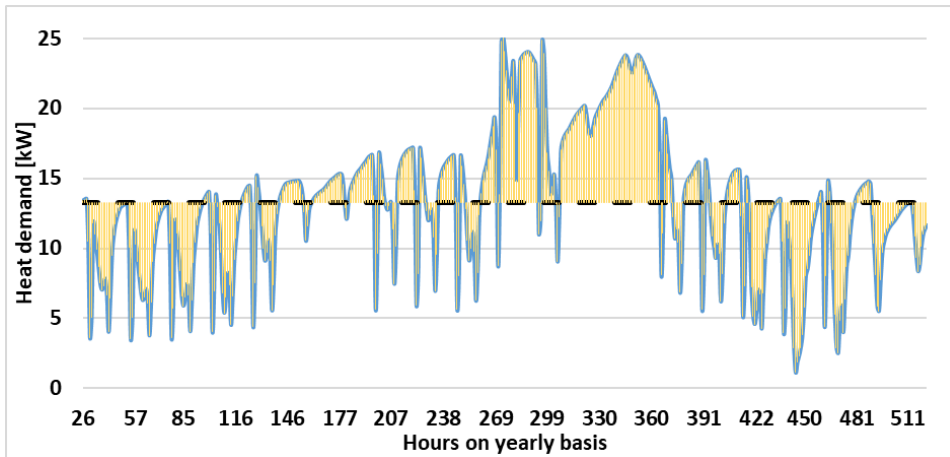


**Figure 4.10:** Heat demand for the coldest 3-week period in January.

It can be observed in Fig. 4.10 that there is an extensive period of high heat demand between 270 h and 362 h. To cover this heat demand without any charging in between, the LHS system must be able to store 400 kWh and 667 kWh of energy fully charged for a heat pump output of respectively 16.2 kW and 13.27 kW. In addition to be able to store enough energy for the periods of high heat demand, the LHS system must be able to transfer enough heat corresponding to the difference between the heat pump output and the peak heat demand. This amounts to a LHS system maximum heat transfer rate of 8.91 kW and 11.84 kW for a heat pump output of respectively 16.2 kW and 13.27 kW. The required average heat transfer output of the LHS system during the extensive period of high heat demand described above is 4.4 kW and 7.33 kW for a heat pump output of respectively 16.2 kW and 13.27 kW. Table 4.4 summarizes these values for the different scenarios.

**Table 4.4:** LHS system requirements for different heat pump power outputs.

Description	$P_{\text{heat pump}}$	
	13.27 kW	16 kW
Heat storage requirement during 3-week period	667 kWh	400 kWh
Maximum LHS system heat transfer rate	11.84 kW	8.91 kW
Average LHS heat transfer rate during period of high heat demand	7.33 kW	4.44 kW

The physical constraints of the LHS system (LHS-1), described in Table 4.2 in Section 4.2.4, restrict the maximum theoretical heat storage capacity of the unit to 325 kWh, which is lower than the requirements in Table 4.4. There will be an additional unit, LHS-2, shown in Fig. 4.3 to help deliver enough heat during critical periods of high heat demand. District heating, described in Section 4.2.1, will also be available to charge the LHS unit faster, due to higher temperatures than the heat pump output.

# 5 — Dynamic System Model

## 5.1 Model Description

To investigate the transient behaviour of charging and discharging the LHS unit, a heat exchanger model using PCM for heat storage has been developed in the modeling and simulation software Dymola [11]. Dymola allows dynamic modeling of thermal systems with variable inputs. It is based on the open, object-oriented modeling language Modelica [28]. The specific heat exchanger model was developed using existing "TIL" libraries from expert thermodynamic model developers at TLK-Thermo GmbH [42]. The model is based on a solid-liquid plate fin-and-tube heat exchanger using PCM for TES custom made by TLK-Thermo GmbH. This LHS model is unique as there is only one mass flow present, for the heat transfer fluid (HTF). The required input parameters for the model are listed in Section 5.3. The LHS model consists of tubes and plate fins running through a tank filled with PCM. Heat transfer rates are calculated from the HTF to the PCM through the tube walls and plate fins. The dimensions of the tank are 1.5-m-high, 1.4-m-wide and 2.5-m-long. To be able to operate the LHS system during peak periods (e.g. cold days), the LHS unit should be fully charged in advance. The control strategy involves to fully charge the LHS unit during off-peak hours, typically 10 hours during the night or during warmer days since the storage capacity enable several days worth of heat demand in the coldest days. The LHS model enables the evaluation of the heat transfer area required to be able to fully charge the system in a predetermined number of hours, assuming a HTF inlet temperature of 40 °C as it can be delivered by the heat pump in off-peak hours. Note that this is the most critical case for charging processes since the connection to district heating enables quicker charge at 45 °C. Fig. 4.2 shows the setup of the LHS system model in Dymola. At the top we find the SIM-block which provides relevant material data and properties for the HTF and the PCM. The top left blocks represent the file reader tool to provide transient input data from external files for dynamic simulations. The heat exchanger block is in the middle of the model with associated mass flow input and pressure output. The blocks in the bottom part of the model are for performance analysis. Fig. 5.2 shows the configuration parameters of the fin and tube heat exchanger model.

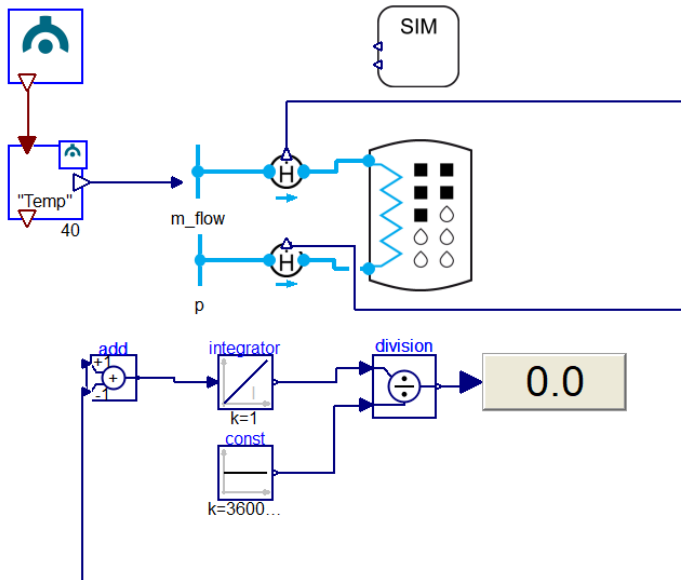


Figure 5.1: PCM heat exchanger model in Dymola.

## 5.2 Model Assumptions

The following assumptions are made for the numerical model:

- Heat transfer coefficient between HTF and inner pipe wall are calculated using combined linear Gnielinski Dittus-Boelter correlation for turbulent flow [17][14].
- No heat transfer by natural convection from fin surface to PCM.
- Swamee-Jain correlation for friction factor to calculate HTF pressure drop through the heat exchanger [24].
- 1-D Schmidt approximation for fin efficiency [37].
- Hysteresis effects are not accounted for in the PCM.
- No heat loss through tank wall.
- The PCM phase changes are complete during charging/discharging processes (no partial load).



### 5.3 Input Parameters

The input parameters and initial parameters for the LHS system model are listed in Tab. 5.1 and Tab. 5.2. Fig. 5.2 shows an illustration of a plate fin-and-tube heat exchanger with associated variable parameters.

**Table 5.1:** Parameters for the PCM heat exchanger model.

<b>Parameter</b>	<b>Unit</b>
Tank height	[m]
Tank width	[m]
Tank depth	[m]
Number of serial tubes	[-]
Number of parallel tubes	[-]
Tube wall thickness	[m]
Tube inner diameter	[m]
Fin thickness	[m]
Fin pitch	[m]
Discretization along the HTF pipe	[-]
Discretization in depth direction from pipe center to PCM	[-]
Inlet HTF (water) temperature	[°C]
Mass flow rate	[ $\frac{kg}{s}$ ]
PCM material properties	[-]
Heat exchanger material properties	[-]

**Table 5.2:** Parameters for initialization of the PCM heat exchanger model.

<b>Parameter</b>	<b>Unit</b>
HTF initial temperature	[°C]
PCM initial temperature	[°C]
Heat exchanger initial temperature	[°C]

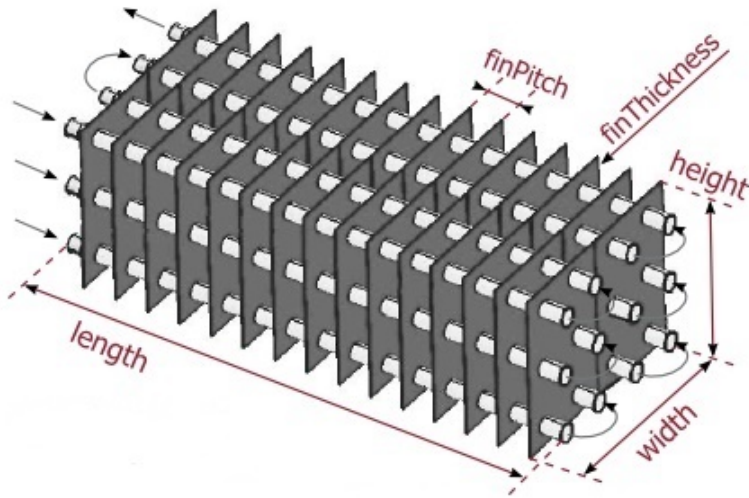


**Figure 5.2:** Illustration of fin and tube heat exchanger geometry.

## 5.4 Discretization

The PCM heat exchanger model, seen in the middle part of Fig. 5.1, is made up of three different type of cells. The PCM (SLE cell) is connected to the liquid cell through wall cells, that represent the HTF pipe and fins. This is shown in Fig. 5.3

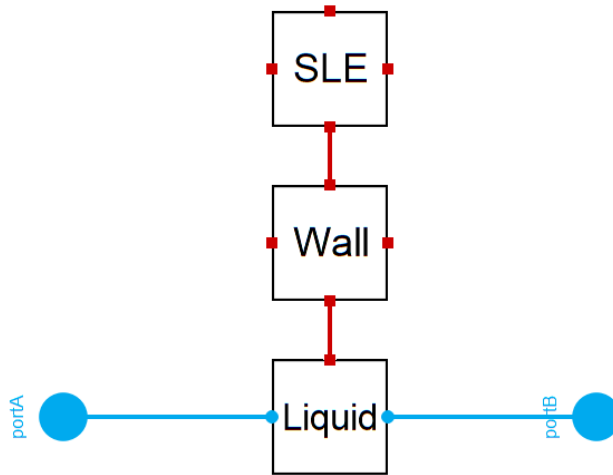


**Figure 5.3:** Internal structure of PCM heat exchanger model.

The discretization of the cells is done in two directions, axially along the HTF pipe flow and radially from the HTF to the PCM, perpendicular to the pipe flow. Fig. 5.4 shows the two different discretizations.

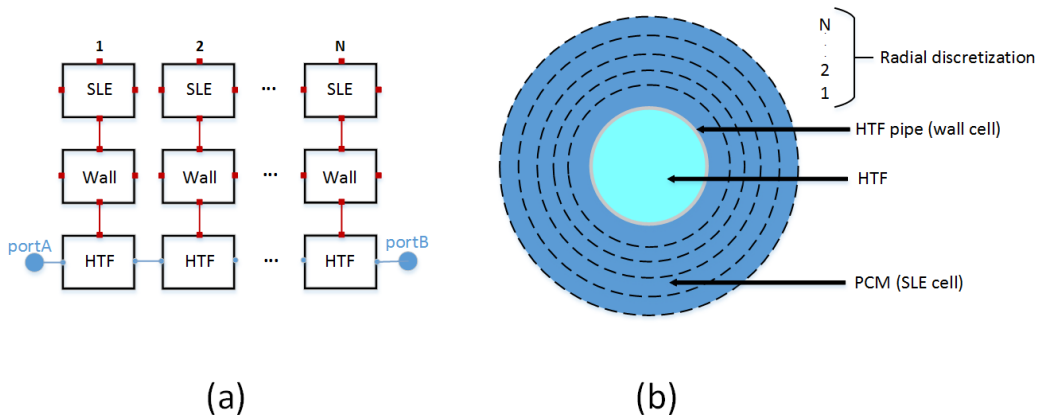


**Figure 5.4:** Discretization of the heat exchanger model: Axially along the heat exchanger (a) and radially (b).

## 5.5 Model output

There is a range of data calculated in the model that is available post-simulation. The parameters chosen for results and discussion are the following:

- HTF inlet temperature [ $^{\circ}\text{C}$ ]
- HTF outlet temperature [ $^{\circ}\text{C}$ ]
- Mass of PCM in heat exchanger [kg]
- Liquid fraction
- Heat transfer rate (enthalpy difference between HTF inlet and outlet) [W]
- Average heat transfer coefficient on the HTF side [ $\frac{\text{W}}{\text{m}^2 \cdot \text{K}}$ ]
- Pressure drop between HTF inlet and outlet [bar]
- PCM temperature at inlet cell [ $^{\circ}\text{C}$ ]
- PCM temperature at outlet cell [ $^{\circ}\text{C}$ ]

In addition, there was done a change to the model to include the average PCM temperature. This was done by calculating the arithmetic average of the PCM temperature in each PCM discretization cell along the heat exchanger.

## 5.6 Validification of Model

TLK has validated the model through experiments not available to the public (Appendix A). To further validate the PCM heat exchanger model, experimental measurement data will be compared to simulated results using the model. The experimental measurement data are from two different scientific publications on experimental investigation of latent heat energy storage in a finned tube heat exchanger [33] [25]. The experiments were reproduced in the PCM heat exchanger model by inserting identical values for the heat exchanger geometry, HTF temperature and by creating an artificial PCM with identical thermal properties to those used in the experiments. Fig. 5.5 shows the experimental and simulated data for the discharge of a latent heat TES. The melting of the PCM is done at constant HTF inlet temperature,  $T_i = 10^{\circ}\text{C}$ . Comparison of the data shows that the model effectively predicts the PCM temperature and time needed for complete solidification of the material.

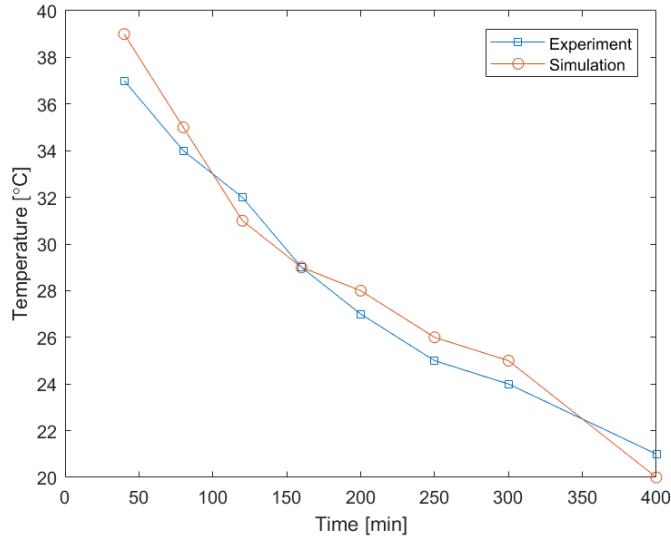


**Figure 5.5:** Simulation and experimental data for discharge of PCM TES.

Fig. 5.6a and Fig. 5.6b show the simulation and experimental results from the charging and discharging of a PCM finned-tube heat exchanger containing a PCM with a melting of  $35^{\circ}\text{C}$  and solidification temperature of  $35^{\circ}\text{C}$ . The HTF, water, is introduced at constant mass flow and temperature ( $60^{\circ}\text{C}$ ) until the discharging process is initiated by changing the HTF temperature to  $10^{\circ}\text{C}$ . The model predicts the final temperatures during melting and solidification well with respect to time. However it can be observed that the model predicts an isothermal phase change process, whereas the experimental measurements show that the phase change happens over a larger temperature range. The reason for this is because the temperature is homogeneously distributed in the PCM volume for the simulation but not in reality. In the experiments, there are local gradients of temperature and additional heat losses leading to non-homogeneous temperature distribution within the PCM and lower PCM temperature at the end than the HTF temperature.

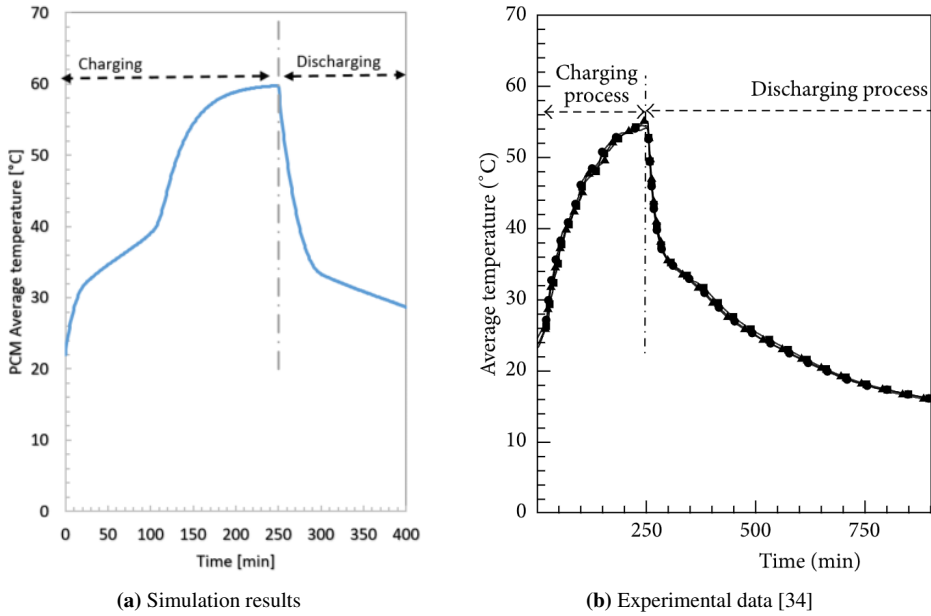


**Figure 5.6:** PCM temperature development during charging/discharging of a fin and tube TES system.

# 6 — Results and Discussion

In this chapter, a parameterization study is conducted in order to identify the main parameters that influence the transient response and the heat storage capacity of the LHS unit. From initial simulations, a base case LHS unit design is defined which will be used for comparison during the parameterization. The base case consist of the following parameters:

**Table 6.1:** Base case heat exchanger parameters.

Parameter	Value	Unit
HTF mass flow rate	2	[ $\frac{kg}{s}$ ]
Number of pipes	225	[-]
Number of serial tubes	15	[-]
Number of parallel tubes	15	[-]
HTF tube inner diameter	10	[mm]
Tube wall thickness	2.5	[mm]
Fin pitch	20	[mm]
Fin thickness	1	[mm]
Number of separate flows (see Fig. 4.8)	1	[mm]

The heat exchanger consists of 225 pipes, arranged 15 x 15 across a transversal section, along the longitudinal axis. The simulations are performed over a sufficiently long time period to allow for complete melting or solidification of the PCM. The main focus for the simulations will be the time required for complete phase change. The preliminary simulations, resulting in the base case design, show that the heat transfer rates are sufficient when compared to the heat demand discussed in Chapter 4, Section 4.3. For the charging processes, the initial temperature is 30°C in the whole LHS unit and the HTF inlet temperature is 40°C. For the discharging processes, the initial temperature is 40°C for the whole LHS unit and the HTF inlet temperature is 30°C. Complete charging will be assumed for an average PCM temperature equal to the HTF inlet temperature. CT37 is used as PCM for all simulations, its thermal properties are listed in Tab. 4.2, Section 4.2.4.

## 6.1 Variable Fin Pitch

Three scenarios are simulated with fin pitches of, respectively, 1, 2 and 4 cm, in the heat exchanger geometry for a constant HTF mass flow of 2 kg/s. Fig. 6.1 and Fig. 6.2 shows the simulation results for one charging process with the tested fin pitches. Fig. 6.1 shows the average PCM temperature throughout the LHS unit. The charging or discharging time is defined here as the time required for the average temperature of the PCM in the LHS

unit to reach the HTF inlet temperature. By reducing the fin pitch from 4 cm to 1 cm, the charging time is reduced from ca. 16 h to 9 h. This is mainly because of the increased surface heat transfer area from the increased quantity of fins, and because the shorter fin pitch also reduces the PCM volume in the LHS unit by 7 %. Fig. 6.2 shows the PCM liquid fraction and heat flow from the PCM to the HTF during the melting process. Heat transfer flows are initially high due to the larger temperature differences driving the heat transfer. They rapidly decrease within the sensible heat transfer region, until the heat flows stabilize when reaching the latent heat transfer region for fin pitches of 1 cm and 2 cm. The fin pitch of 4 cm does not yield such a sharp change during phase change.

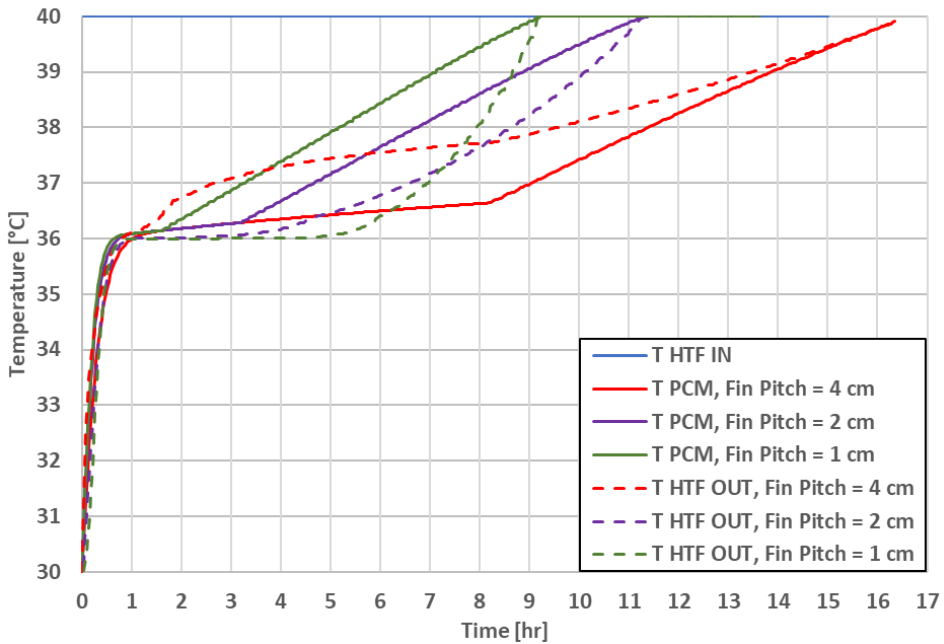


**Figure 6.1:** Temperature of HTF at inlet and outlet, PCM average temperature during charging.



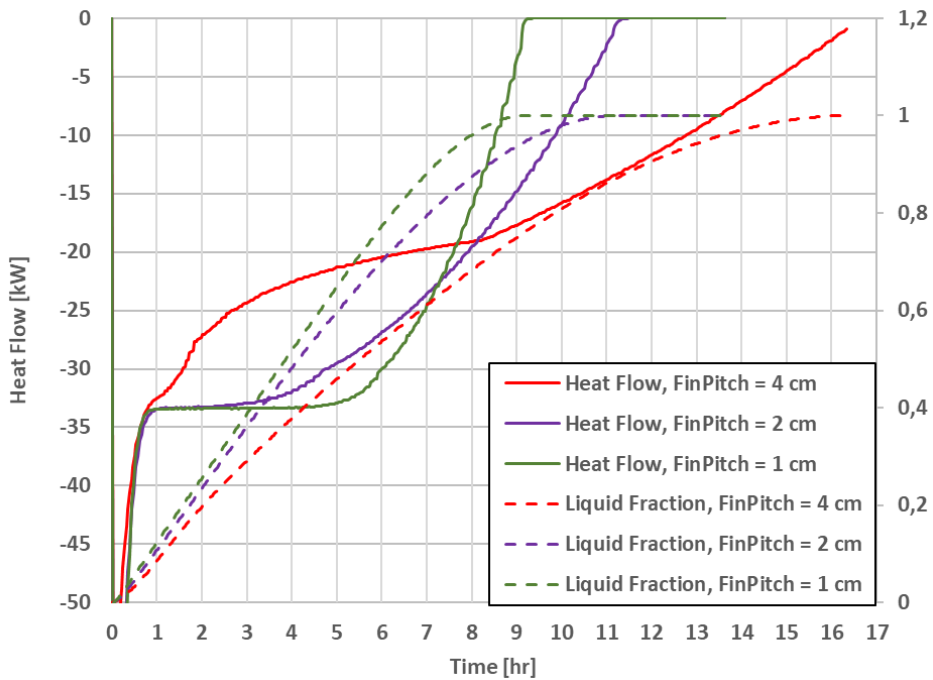


**Figure 6.2:** Heat flow from HTF to PCM and PCM liquid fraction during charging.

Fig. 6.3 and Fig. 6.4 shows the results of the discharging simulations for the tested fin pitches. As shown in Fig. 6.3, a fin pitch of 1 cm yields an HTF outlet temperature almost constant at  $36^{\circ}\text{C}$  for 2 hours, which is optimal for the steady operation of the heat pump. Increasing the fin pitch results in steadily decreasing HTF outlet temperature during discharging. Fig. 6.4 shows that reducing the fin pitch provides higher and more constant heat flows in the latent heat transfer region, ultimately leading to shorter discharging times. According to the simulations, a fully charged system stores respectively 293 kWh, 286 kWh and 271 kWh for a fin pitch of 4 cm, 2 cm and 1 cm. This yields average heat transfer rates of ca. 35 kW, 44 kW and 50 kW for the various fin pitch distances during discharge. These results validate the thermal performance for the proposed design of the LHS system, both in terms of charging times and heat transfer rates during discharge. Charging of the system may occur over night when the building is not in use, typically for a time period of maximum 10 hours. Fig. 6.1 shows that this can be achieved using a fin pitch distance of 1 or 2 cm. Fig. 6.3 confirms that the LHS unit can raise the return temperature of the heating circuit closer to design intake conditions for the heat pump ( $35^{\circ}\text{C}$ ). Fig. 6.4 demonstrates that the LHS unit is able to deliver more than sufficient heat transfer rates, to meet the maximum heat demand in combination with the heat pump.

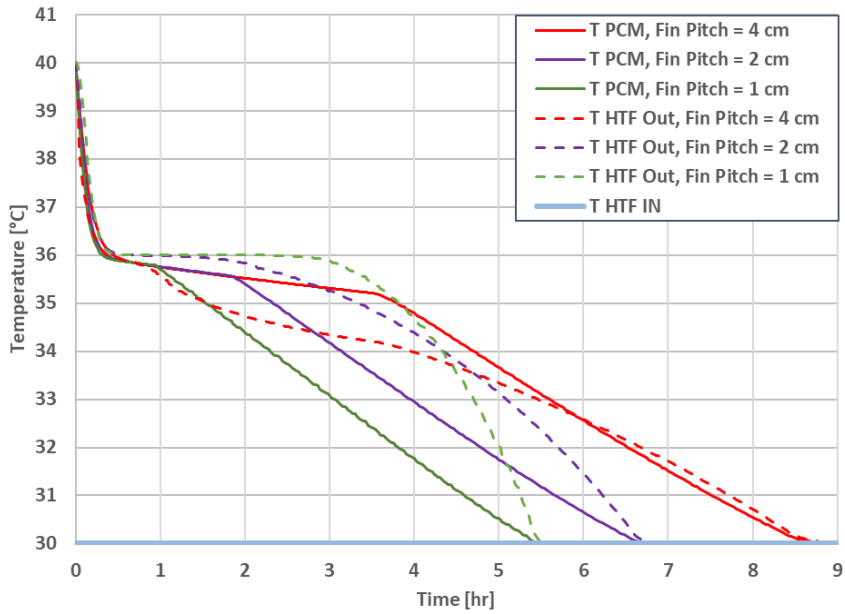


**Figure 6.3:** Temperature of HTF at inlet and outlet, PCM average temperature during discharging.

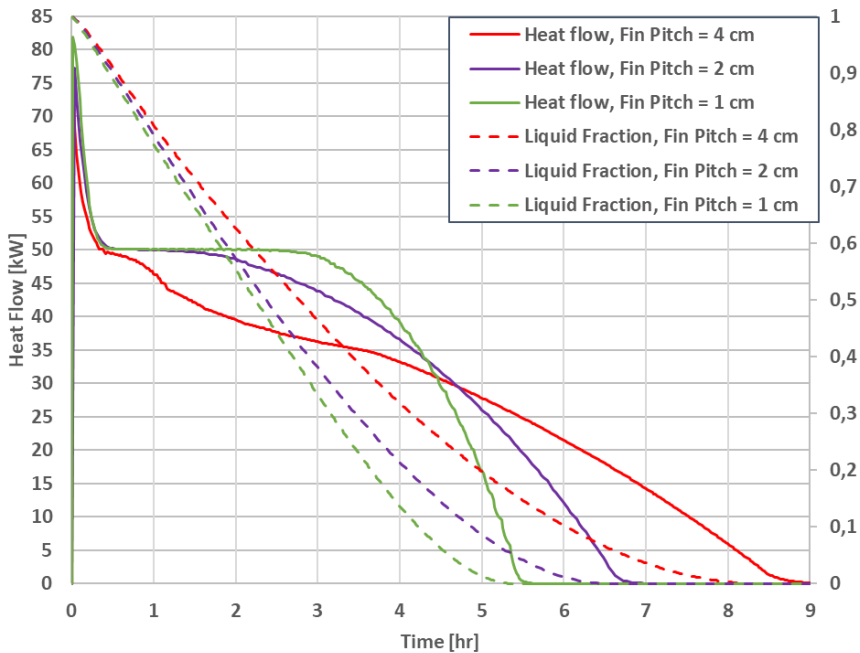


**Figure 6.4:** Heat flow from HTF to PCM and PCM liquid fraction during discharging.

## 6.2 Variable Mass Flow

The next three scenarios are simulated with a variable HTF mass flow rate of respectively 1, 2 and 3 kg/s, for a constant fin pitch of 2 cm. Fig. 6.5 and Fig. 6.6 show the results for a charging and discharging cycle for three different mass flows. The fin pitch is set to 2 cm. A mass flow rate of 1 kg/s gives a complete charging time of 19 hours. The temperature of the HTF at the outlet for this mass flow rate indicates that all heat is transferred from the HTF during the phase change. An increase in mass flow from 1 to 2 kg/s reduces the charging time approximately 8 hours to a total time of 11.2 hours. A further increase in mass flow rate to 3 kg/s reduces the charging time 23 % to 8.6 hours. The reduction in charging time is due to the increased convective heat transfer from the HTF to the pipe wall due to the higher flow rates. Fig. 6.6 presents the equivalent parameter scenario, for a discharging cycle. Complete discharging of the LHS unit is reduced from 11.2 hours to 4.8 hours when changing the mass flow rate from 1 to 3 kg/s. The greatest change in discharging time (40 %) is observed for a mass flow increase from 1 to 2 kg/s.

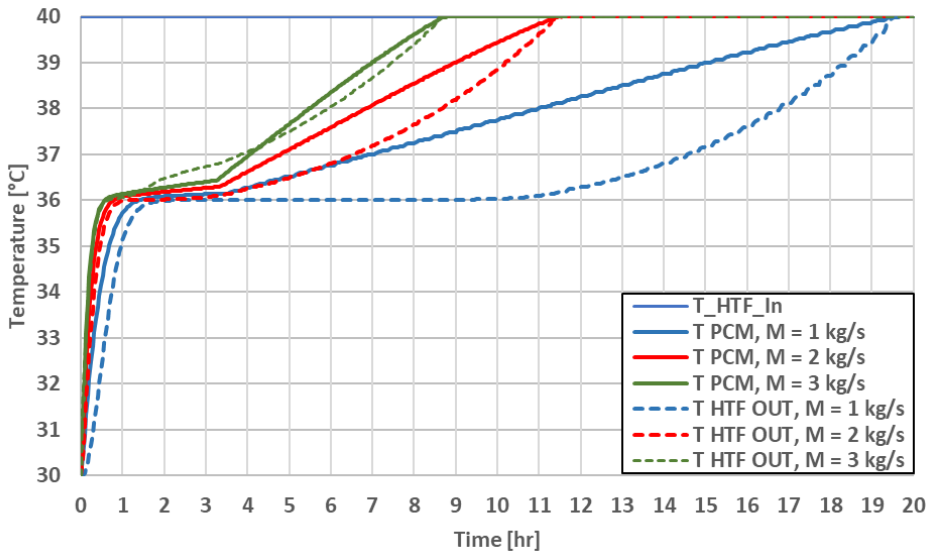


**Figure 6.5:** Temperature of HTF at inlet and outlet, PCM average temperature during charging.

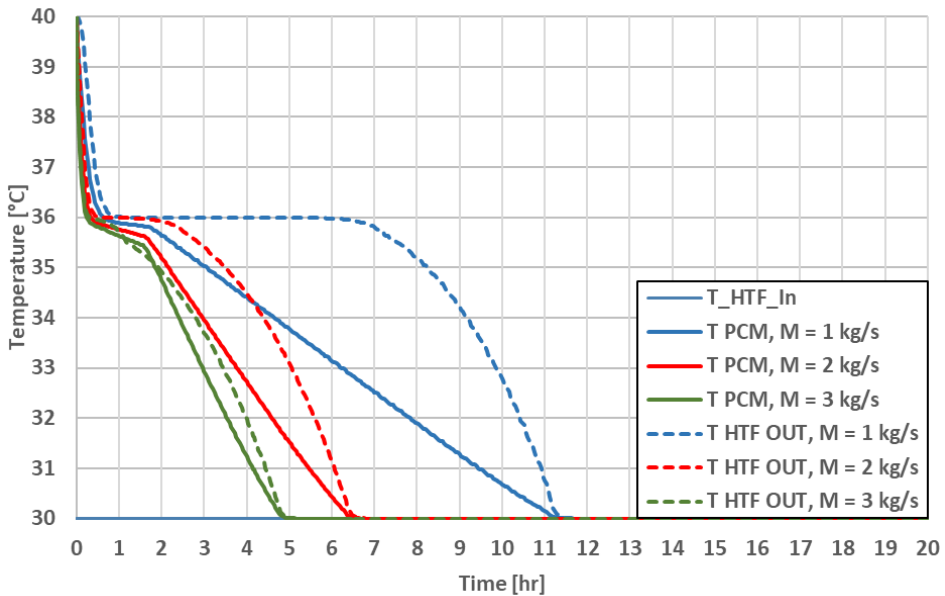


**Figure 6.6:** Temperature of HTF at inlet and outlet, PCM average temperature during discharging.

### 6.3 Variable Fin Thickness

Fig. 6.7 shows the effect of fin thickness on the charging time and on total mass of PCM in the LHS unit. The average PCM temperature development is plotted for each fin thickness with corresponding amount of PCM on the right axis. The charging time is reduced with approximately 3.9 hours with a fin thickness increase from 1 mm to 4mm. This change in fin thickness reduces the amount of PCM in the LHS unit by 734 kg. This reduction in PCM will affect the charging time as there is less PCM in the system to be melted. For an increasing fin thickness, the distance between each fin is reduced, leading to shorter melting distances for the PCM and thus reducing the time required for melting. The greatest reduction in time required for complete charging is observed from a fin thickness increase of 1 mm to 2 mm. The reduction equals a 19.7 % change compared to a charging time reduction of 10 % when increasing the fin thickness further from 2 mm to 3 mm.

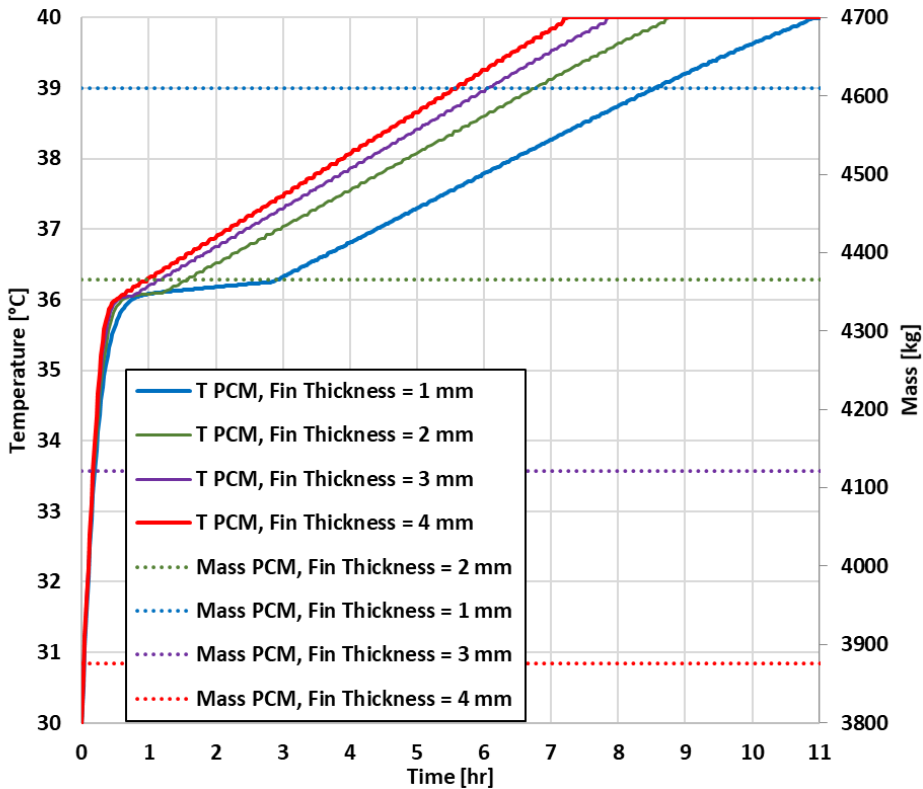


**Figure 6.7:** Average PCM temperature and total amount of PCM in LHS unit during a charging cycle.

## 6.4 Variable Pipe Flow Configuration

The number of separate flows (SF) can be varied for the heat exchanger design. Fig. 4.8, Section 4.2.5 illustrates this. With one single SF (one inlet and outlet), the HTF mass flow rate equals the mass flow rate in the HTF tube. Also, the number of passes required for the HTF to travel through, increases. As the number of SF increases, the mass flow rate and the total length the HTF has to travel through the heat exchanger is reduced for each SF. The actual LHS unit will have 225 tubes. This means it can be designed for one SF passing through the whole heat exchanger 225 times, or 225 SF passing through once. It is assumed for the simulations, that all number of SF are physically possible.

The simulation results for a varying amount of SF during a charging cycle are shown in Fig. 6.8. Simulations were done starting with one SF, then increasing the number of SF up to 175, where the charging time increased abruptly. Increasing the total amount of SF from 1 up to 150 has a relatively moderate effect on the change on the total charging time. The increased charging time (11.07 to 15.1 hours) is mainly due to the reduced heat transfer, owing to reduced mass flow per tube as total number of SF increases. Fig. 6.9 shows the calculated heat transfer coefficient for the HTF (logarithmic) for an increasing number of SF. For 175 SF, the charging time increases by approximately 100 % when compared to the charging time with 150 SF. This can be explained by a flow regime change in the HTF tubes from turbulent to laminar flow as the number of SF are increased beyond 86 ( $Re \approx 4000$ ). Increasing the number of SF beyond 151 gives a Reynolds number below 2300, which is characterized as critical a Reynolds number where the flow becomes laminar [8]. The heat transfer coefficient is reduced greatly from fully turbulent flow to laminar flow, as can be observed in Fig. 6.9. The heat transfer coefficient in the transition phase is unknown and is represented by a straight line.

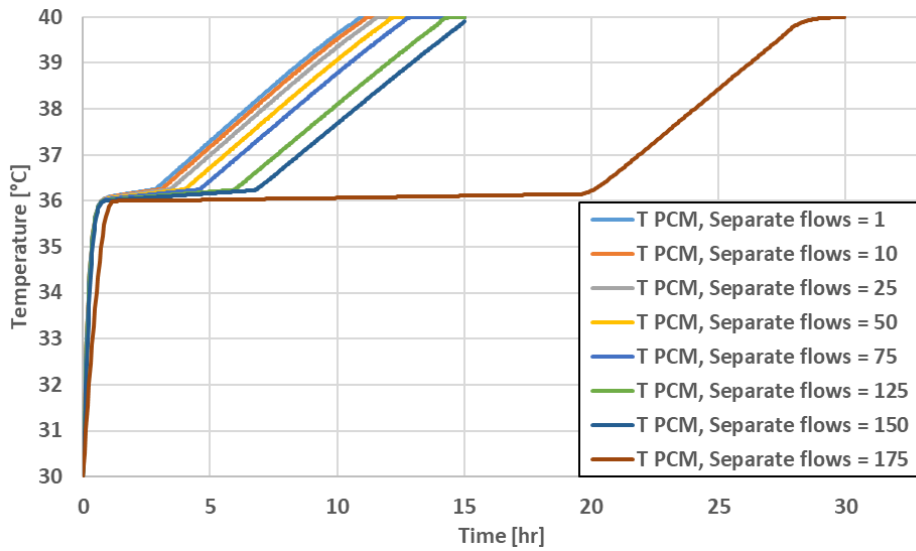


**Figure 6.8:** Average PCM temperature for an increasing number of separate flows during a charging cycle.

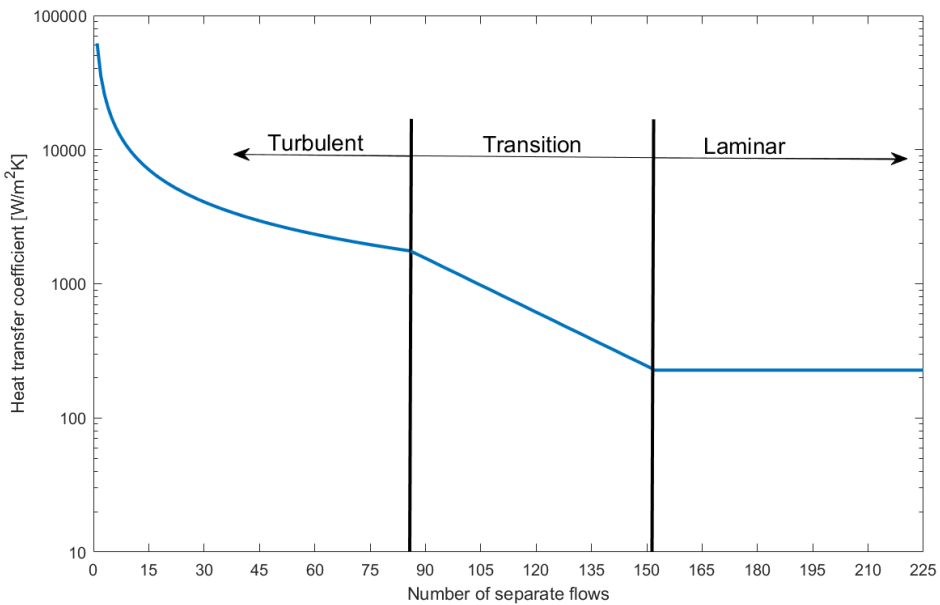


**Figure 6.9:** Calculated heat transfer coefficient for HTF [Appendix C].

Fig. 6.10 shows the calculated and simulated pressure drop (logarithmic) for the HTF

through the heat exchanger. The red line shows the calculated (Matlab) pressure drop using the Swamee-Jain equation [24] to solve the Darcy friction factor. This pressure drop is calculated as if the total HTF tube section is a straight pipe. For the blue line, denoted as total pressure drop, a pressure drop term for the additional pressure drop in bends is included. In order for the HTF to travel through all 225 pipes,  $180^\circ$  bends are included in the heat exchanger. The total amount of bends depends on the number of separate flows. For a SF of 1, there will be 224 bends. For a number of SF of 225, there will be no bends as the HTF is travelling straight through the heat exchanger without any passes. The pressure drop at the entrance and exit headers are also included in the total pressure drop calculations, assuming 0.5 velocity head loss at the entrance and 1 velocity head loss at the exit. When comparing the pressure drop calculations to the simulated pressure drop (heat exchanger model), there is a correlation between the simulated pressure drop and the calculated data assuming a straight pipe. This indicates that the pressure drop model in the heat exchanger model does not account for pressure drop in the HTF pipe bends. The results show that the pressure drop is very large for few separate flows. For 10 SF, the HTF pressure drop is 14.26 bar through the heat exchanger. The number of SF has to be increased to  $\sim 30$  to obtain a pressure drop of 1 bar, according to the total pressure drop calculation. Although the heat transfer coefficient is reduced exponentially (Fig. 6.9), an increase of SF from 1 to 30 does not increase the LHS unit charging time more than 21.6 minutes (3.25 %). This shows that a low amount of SF increases the HTF pressure drop greatly, without reducing charging time by the same magnitude.

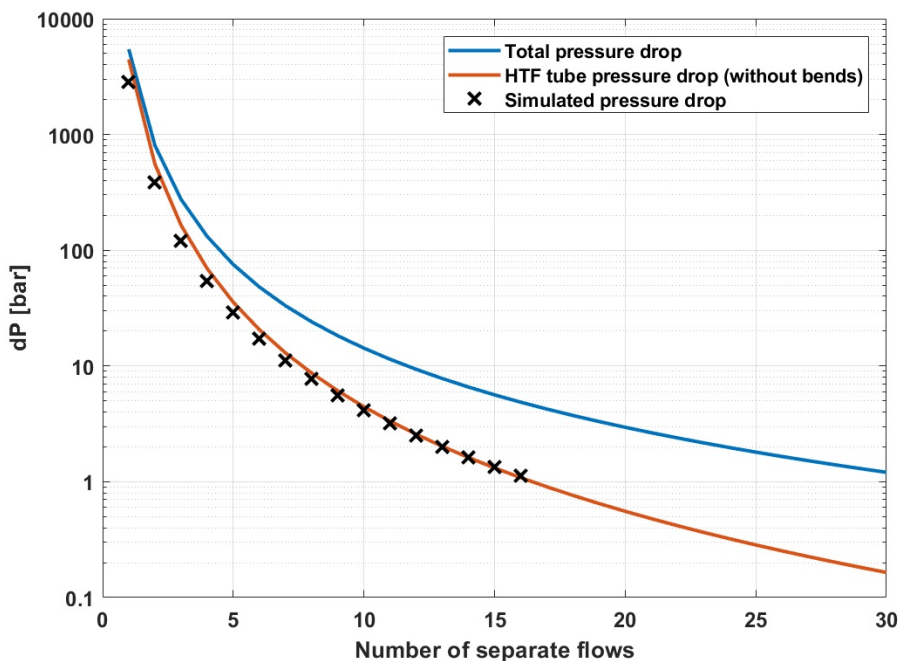


Figure 6.10: Pressure drop for HTF [Appendix D].



## 7 — Conclusion

The purpose of this master's thesis was to assist the design of a compact and effective LHS system to be built in the upcoming ZEB Flexible Laboratory. A literature study on general principles of latent heat storage and general (LHS) design of centralized heating for buildings has been conducted. A Modelica based model for simulating the performance of a latent heat storage (LHS) unit has been built based on a fin-and-tube PCM heat exchanger. The purpose of the model was to provide an understanding of the dynamics of a LHS unit in order to evaluate heat transfer rates and charging/discharging times. The final goal was to dimension a functional system for the ZEB Flexible Laboratory, based on the properties of its heating system and heat demand. Through dynamical modeling, a parameterization study has been completed to investigate how changing various parameters affects the time required for complete melting/solidification of the PCM in the LHS unit. A simple control strategy has been developed for the initiation of charging/discharging of the LHS unit. In addition, a PCM has been chosen, CrodaTherm 37 (CT37), for the LHS unit based on its thermal properties, commercial availability and DSC testing results.

Based on the results from the parameterization study a plate-fin-and-tube design is proposed for the LHS unit with the following properties:

- Unit dimensions [m]:  $1.5 \times 1.4 \times 2.5$  (height  $\times$  width  $\times$  length)
- Number of HTF tubes: 225
- HTF tube inner dimension [m]: 0.01
- HTF tube wall thickness [m]: 0.0025
- Number of separate HTF flows: 45
- Fin pitch [m]: 0.02
- Fin thickness [m]: 0.001
- PCM: CrodaTherm 37
- HTF tube material: Copper
- Fin material: Aluminum
- HTF pump motor power [kW]: 0.3

This LHS unit design allows for a complete charge during 12 hours and is able to transfer enough heat during a discharging cycle to successfully support the heat pump during peak heat demand. This means increasing the return HTF temperature by an average of 4.1 °C for a discharging period of 8 hours. The number of separate HTF flows chosen minimizes the pressure drop remarkably, while not reducing the HTF tube side heat transfer enough to affect charging times excessively.

---

## 7.1 Further work

Due to limitations of time, the dynamic model and the phase of the ZEB Flexible Laboratory project during the thesis work, recommendations for further work are:

- Extend the dynamic model to include varying PCM properties during phase change.
- Extend the dynamic model to include the effects of free convection heat transfer mechanisms between the fins and PCM.
- Use measurement data from the ZEB Flexible Laboratory as input for the dynamic model after the use of the building has commenced to simulate realistic conditions.
- Develop the control strategy for the LHS unit based on measurement data from the ZEB Flexible Laboratory.

# Bibliography

- [1] Agyenim, F., Eames, P., Smyth, M., 2010. Heat transfer enhancement in medium temperature thermal energy storage system using a multitube heat transfer array. *Renewable Energy* 35 (1), 198–207.
- [2] Agyenim, F., Hewitt, N., 2010. The development of a finned phase change material (pcm) storage system to take advantage of off-peak electricity tariff for improvement in cost of heat pump operation. *Energy and Buildings* 42 (9), 1552–1560.
- [3] Agyenim, F., Hewitt, N., Eames, P., Smyth, M., 2010. A review of materials, heat transfer and phase change problem formulation for latent heat thermal energy storage systems (lhtess). *Renewable and sustainable energy reviews* 14 (2), 615–628.
- [4] Bonamente, E., Aquino, A., Cotana, F., 2016. A pcm thermal storage for ground-source heat pumps: Simulating the system performance via cfd approach. *Energy Procedia* 101, 1079–1086.
- [5] Cabeza, L., Martorell, I., Miró, L., Fernández, A., Barreneche, C., 2015. Introduction to thermal energy storage (tes) systems. In: *Advances in Thermal Energy Storage Systems*. Elsevier, pp. 1–28.
- [6] Cabeza, L. F., Castell, A., Barreneche, C., De Gracia, A., Fernández, A., 2011. Materials used as PCM in thermal energy storage in buildings: a review. *Renewable and Sustainable Energy Reviews* 15 (3), 1675–1695.
- [7] Castro, P. P., Selvam, P. K., Suthan, C., 2016. Review on the design of pcm based thermal energy storage systems. *Imperial Journal of Interdisciplinary Research* 2 (2).
- [8] Cengel, Y. A., 2010. *Fluid mechanics*. Tata McGraw-Hill Education.
- [9] Choi, J. C., Kim, S. D., 1992. Heat-transfer characteristics of a latent heat storage system using  $\text{MgCl}_2 \cdot 6\text{H}_2\text{O}$ . *Energy* 17 (12), 1153–1164.
- [10] Croda, 2019. *Crodatherm 37 - Datasheet*. [https://www.crodatherm.com/en-gb/products-and-applications/product-finder/product/1387/CrodaTherm\\_1\\_37](https://www.crodatherm.com/en-gb/products-and-applications/product-finder/product/1387/CrodaTherm_1_37).
- [11] Dassault Systèmes, 2019. *Dymola systems engineering*. <https://www.3ds.com/products-services/catia/products/dymola/>.
- [12] de Gracia, A., Cabeza, L. F., 2015. Phase change materials and thermal energy storage for buildings. *Energy and Buildings* 103, 414–419.
- [13] DiBK, 2019. *Tek17*. <https://dibk.no/byggereglene/byggteknisk-forskrift-tek17/15/ii/15-5/>.

- 
- [14] Dittus, F., Boelter, L., 1985. Heat transfer in automobile radiators of the tubular type. *International Communications in Heat and Mass Transfer* 12 (1), 3–22.
- [15] Esen, M., 2000. Thermal performance of a solar-aided latent heat store used for space heating by heat pump. *Solar energy* 69 (1), 15–25.
- [16] Esen, M., Durmuş, A., Durmuş, A., 1998. Geometric design of solar-aided latent heat store depending on various parameters and phase change materials. *Solar energy* 62 (1), 19–28.
- [17] Gnielinski, V., 1976. New equations for heat and mass transfer in turbulent pipe and channel flow. *Int. Chem. Eng.* 16 (2), 359–368.
- [18] Gong, Z.-X., Mujumdar, A. S., 1997. Finite-element analysis of cyclic heat transfer in a shell-and-tube latent heat energy storage exchanger. *Applied Thermal Engineering* 17 (6), 583–591.
- [19] Hamada, Y., Ohtsu, W., Fukai, J., 2003. Thermal response in thermal energy storage material around heat transfer tubes: effect of additives on heat transfer rates. *Solar Energy* 75 (4), 317–328.
- [20] Hirmiz, R., Teamah, H., Lightstone, M., Cotton, J., 2019. Performance of heat pump integrated phase change material thermal storage for electric load shifting in building demand side management. *Energy and Buildings* 190, 103–118.
- [21] Horbaniuc, B., Dumitrascu, G., Popescu, A., 1999. Mathematical models for the study of solidification within a longitudinally finned heat pipe latent heat thermal storage system. *Energy Conversion and Management* 40 (15-16), 1765–1774.
- [22] Jacobsen, T., Andresen, I., 2018. Zeb flexible laboratory.
- [23] Jokiel, M., Kauko, H., Schlemminger, C., Hafner, A., Claussen, I. C., 2017. Phase change material thermal energy storage for a large scale ammonia chiller/heat pump system. Interactive effects of ammonia and oxygen on growth and physiological status of juvenile Atlantic cod (*Gadus morhua*).
- [24] Kijjarvi, J., 2011. Darcy friction factor formulae in turbulent pipe flow. *Lunowa Fluid Mechanics Paper* 110727, 1–11.
- [25] Koukou, M. K., Vrachopoulos, M. G., Tachos, N. S., Dogkas, G., Lymperis, K., Stathopoulos, V., 2018. Experimental and computational investigation of a latent heat energy storage system with a staggered heat exchanger for various phase change materials. *Thermal Science and Engineering Progress* 7, 87–98.
- [26] Kristjansson, K., Næss, E., Skreiberg, Ø., 2016. Dampening of wood batch combustion heat release using a phase change material heat storage: Material selection and heat storage property optimization. *Energy* 115, 378–385.
- [27] Larsen, A. F., 2017. Timeverdier for effekt for 1700 m2 bygg [Microsoft Excel spreadsheet]. Link Arkitektur.
-

- 
- [28] Modelica, 2019. Modelica and the Modelica Association. <https://www.modelica.org/>.
- [29] Moreno, P., Castell, A., Solé, C., Zsembinszki, G., Cabeza, L. F., 2014. Pcm thermal energy storage tanks in heat pump system for space cooling. *Energy and Buildings* 82, 399–405.
- [30] Oró, E., De Gracia, A., Castell, A., Farid, M., Cabeza, L., 2012. Review on phase change materials (PCMs) for cold thermal energy storage applications. *Applied Energy* 99, 513–533.
- [31] Pavlov, G. K., Olesen, B. W., 2011. Building thermal energy storage-concepts and applications.
- [32] PCM Products, 2019. [http://www.pcmproducts.net/Phase\\_Change\\_Material\\_Products.htm](http://www.pcmproducts.net/Phase_Change_Material_Products.htm), Accessed: 2019-03-18.
- [33] Rahimi, M., Ranjbar, A., Ganji, D., Sedighi, K., Hosseini, M., 2014. Experimental investigation of phase change inside a finned-tube heat exchanger. *Journal of Engineering* 2014.
- [34] Rahimi, M., Ranjbar, A., Ganji, D., Sedighi, K., Hosseini, M., Bahrapoury, R., 2014. Analysis of geometrical and operational parameters of pcm in a fin and tube heat exchanger. *International Communications in Heat and Mass Transfer* 53, 109–115.
- [35] Regjeringen, 2017. Innfører forbud mot bruk av mineralolje til oppvarming av bygninger fra 2020. <https://www.regjeringen.no/no/aktuelt/oljefyr/id2556868/>, Accessed: 2019-02-12.
- [36] Rubitherm, 2019. <https://www.rubitherm.eu/en/productCategories.html>, Accessed: 2019-03-18.
- [37] Schmidt, T., 1945. La production calorifique des surfaces munies dailettes. *Annexe Du Bulletin De LInstitut International Du Froid*, Annexe G-5.
- [38] Sevault, A., Kauko, H., Bugge, M., Banasiak, K., Haugen, N. E. L., Skreiberg, Ø., 2017. Phase change materials for thermal energy storage in low- and high-temperature applications: a state-of-the-art.
- [39] Sharma, A., Tyagi, V. V., Chen, C., Buddhi, D., 2009. Review on thermal energy storage with phase change materials and applications. *Renewable and Sustainable energy reviews* 13 (2), 318–345.
- [40] Soibam, J., 04 2018. Numerical investigation of a heat exchanger using phase change materials (PCMs) for small-scale combustion appliances.
-

- 
- [41] Splide, D., K. Lien, S., B. Ericson, T., H. Magnussen, I., 2018. Rapport - Strømforbruk i Norge mot 2035.
- [42] TLK-Thermo GmbH, 2019. Til suite thermal systems. <https://www.tlk-thermo.com/index.php/en/software-products/til-suite>.
- [43] Velraj, R., Seeniraj, R., Hafner, B., Faber, C., Schwarzer, K., 1999. Heat transfer enhancement in a latent heat storage system. *Solar energy* 65 (3), 171–180.
- [44] Youssef, W., Ge, Y., Tassou, S., 2017. Effects of latent heat storage and controls on stability and performance of a solar assisted heat pump system for domestic hot water production. *Solar Energy* 150, 394–407.
- [45] Zhang, Y., Wang, X., Zhang, Y., Zhuo, S., 2016. A simplified model to study the location impact of latent thermal energy storage in building cooling heating and power system. *Energy* 114, 885–894.

# Appendices

## A Validation correspondence with TLK-Thermo GmbH

---

Hi Fabian Bøhmer,

enclosed you find a short model documentation.

The model is validated with experimental data within different confidential projects.

Additional SLE fluids can be implemented in TILMedia 3.5 by the user as follows:

TILMedia\Internals\SLEMedium

here you find an implementation using Modelica language that should be

hopefully understandable for a user.

Property data for SLE media with phase change temperature 30/40 degC might be available

from Rubitherm <https://www.rubitherm.eu/index.php/produktkategorie/organische-pcm-rt>

or other manufacturers.

Best regards

Sven Försterling

---

## B Scientific publication

Submitted 15.05.2019 for the 1st Nordic ZEB+ conference on Zero Emission and Plus Energy Buildings.

### Latent heat storage for centralized heating system in a ZEB living laboratory: integration and design

Alexis SEVAULT<sup>1</sup>, Fabian BÖHMER<sup>2</sup>, Erling NÆSS<sup>2</sup>, Liang WANG<sup>1</sup>

<sup>1</sup> SINTEF Energy Research, P.O. Box 4761 Torgarden, NO-7465 Trondheim, Norway

<sup>2</sup> NTNU Department of Energy and Process Engineering, Trondheim, 7491, Norway

Alexis.Sevault@sintef.no

**Abstract.** The ZEB Flexible Laboratory project, coordinated by SINTEF and NTNU, aims at building a ZEB (Zero Emission Building) in Trondheim (Norway) in 2019, to be used both as office building and living laboratory. An innovative latent heat storage (LHS) unit using phase change material (PCM) will be integrated in the centralized heating system. The LHS unit will be able to store excess heat from various heat sources connected to the heating system, when they are not required for space heating. One challenge is to make use of the full potential of the PCM latent heat to have a compact and effective unit, while the unit itself should have a low associated CO<sub>2</sub>-footprint. The LHS system consists of two units designed for a total heat storage capacity of 0.6 MWh, corresponding to the heat needed on top of the heat pump to cover for up to 3 consecutive days in the coldest period of the year, with a maximum combined effect of 26 kW. A bio-based wax is used as PCM with melting temperature 37 °C and measured latent heat 198 kJ/kg. Dynamic system modelling is used to support the design of the LHS unit and ensure sufficiently high heat transfer rates.

**Keywords.** Phase Change Materials, PCM, Thermal Energy Storage, Heat Storage, Building, Centralized Heating system.

#### 1. Introduction

##### 1.1. Background

The ZEB Flexible Laboratory project, coordinated by SINTEF and NTNU, aims at building a ZEB (Zero Emission Building) in Trondheim (Norway) in 2019, to be used both as office building and living laboratory [1]. The building will rely on innovative technologies, both regarding building materials and energy system. One technology to be implemented and tested in the centralized heating system of the building will be a latent heat storage (LHS) unit using a phase change material (PCM). The LHS unit will be integrated in the low-temperature heating system centred around a heat pump providing hot water for space heating. An essential asset of the LHS unit is to be able to provide high heat storage capacity and heat effect within the narrow temperature range offered by low-temperature heating. During hours of low heat demand, the LHS unit will be able to store excess heat. During high demand, the stored heat will be released either to provide heat directly to the heating circuit or to support the heat pump by compensating for a drop of return temperature below the optimal intake temperature. Since such LHS technology is not commercially available yet, an experimental unit has to be custom-designed following the best integration path in the heating system.



---

### 1.2. Objective

The main objectives of the present study are: (1) to determine the best integration scenario for the LHS unit in the centralised heating system of the ZEB Flexible Laboratory; (2) to dimension the LHS unit according to the building energy demand, while selecting the most appropriate PCM; and (3) to model the dynamic thermal performance of the designed LHS unit to validate its general design.

### 1.3. Literature review

A well-known challenge with using PCM for thermal energy storage is the poor thermal conductivity for available PCMs, limiting heat transfer rates [2, 3]. Comprehensive work has been done to increase the heat transfer rates within LHS systems by utilizing heat transfer enhancement techniques in numerical investigations and in experimental setups. However, only a few full-scale active LHS systems are in operation, making it challenging to document the potential upsides of coupling a LHS system to a heat pump for peak shaving and heating purposes.

Hirmiz et al. [4] studied the integration of LHS systems into heat pump systems to improve the demand side flexibility and, ideally, the strategy for the LHS system to cover the complete heat demand during peak periods. By utilizing a TRNSYS numerical model, it was concluded that a LHS system can completely offset peak heat demand periods within 2 to 6 hours, reducing peaks in the power grid. Through modelling and measurement data analysis, Jokiel et al. [5] evaluated a LHS system installed to reduce the required chiller capacity for three ammonia chillers/heat pumps covering the base load for heating/cooling at the Bergen University College (Norway). A dynamic system model was developed using Modelica [6] to better understand the dynamics of melting and solidification of the PCM. The model proved to correctly predict the measured data, within an acceptable accuracy, especially regarding the accumulated values of absorbed and released heat.

Bonamente et al. [7] studied the potential for system optimization in an existing ground-source heat pump heating system by implementing a TES unit. Computational fluid dynamic calculations were carried out and validated against measured data using two TES solutions: one using water as storage medium, and the other using PCM. Results showed that the COP of the system was increased from 2.9 to 3.2 and 3.4 for, respectively, heating and cooling modes when using water as TES medium. By using a PCM, the system COP was increased to 4.13 and 5.89 for, respectively, heating and cooling modes. In addition, the total volume of the PCM thermal storage was 10 times more compact compared to the water tank system making it more suitable for indoor installation and use.

Shifting the cooling load during simulated summer conditions was experimentally tested by Moreno et al. [8] by coupling a TES system to a heat pump. Thermal behaviour for the TES system was evaluated for cold storage and for space cooling. Two different TES configurations were tested, one using water and the other using PCM. The latter configuration utilized macro-encapsulated PCM with a phase change temperature of 10 °C. It was concluded that PCM storage is favourable to water storage. With identical volumes, the PCM tank was able to store 35.5 % more cold energy on average compared to the water storage tank. Other results indicated that by increasing the heat transfer rate for the PCM storage, it could store 14.5 % more cold energy, while delivering an acceptable indoor temperature for a 20.65 % longer duration compared to the water storage.

## 2. Integration of LHS unit

### 2.1. Centralized heating system

The building heating system is centralized and originally relies on a 25-kW heat pump system and several heat sources and heat sinks along the hot water heating circuit. The selected heat pump system is designed to provide a temperature lift on the hot side from 35 °C to 40 °C. Besides the heat pump, heat from the local district heating is used as heat source for the building, providing hot water at 45 °C. Throughout the heating circuit, preheating of domestic hot water, room radiators and heat exchangers providing heated air for ventilation are used as heat sinks to heat up the building. Additional components enabling research experiments in the different rooms of the buildings are also

planned but constitute minor heat sinks and heat sources on the heating circuit and thus are out of the scope of the present study. Without the LHS unit, the heat pump is meant to cover the maximum heat demand of the building, calculated to ca. 26 kW, necessary to maintain all rooms in the building at a comfortable temperature on the coldest days of the year in Trondheim (Norway). Using the LHS unit to support peak heating demands, the size and nominal effect of the heat pump can be significantly reduced, so that it operates more effectively.

## 2.2. LHS unit integration

Among the possible scenarios to integrate the LHS unit in the centralized heating system, the integration enabling thermal buffering to support the heat pump was selected (see Figure 1). Depending on the heating demand in the building, the return temperature of the heating loop might be lower than 34 °C, and thus require additional power from the heat pump to sustain 40 °C as outlet temperature. Integrating the LHS unit downstream from the heat pump, with the option to circulate the return water through it or not, provides the opportunity to both charge and discharge the LHS unit, while smoothing the effect demand from the heat pump. Charging the LHS unit occurs when the heating demand is low, using 40 °C as inlet temperature, as it is generated by the heat pump. Using a PCM with phase change temperature within 34-37 °C, return water at lower temperature than 34 °C can circulate through the charged LHS unit and be heated up before entering the heat pump. Additionally, the LHS unit can be directly charged using the district heating loop providing hot water at 45 °C. Note that, as shown in Figure 1, two LHS units (LHS-1 and LHS-2) are integrated in the heating system, to ultimately allow for research experiments using various heat exchanger designs and test the thermal performance of several PCM. The present study focuses only on the design of LHS-1.

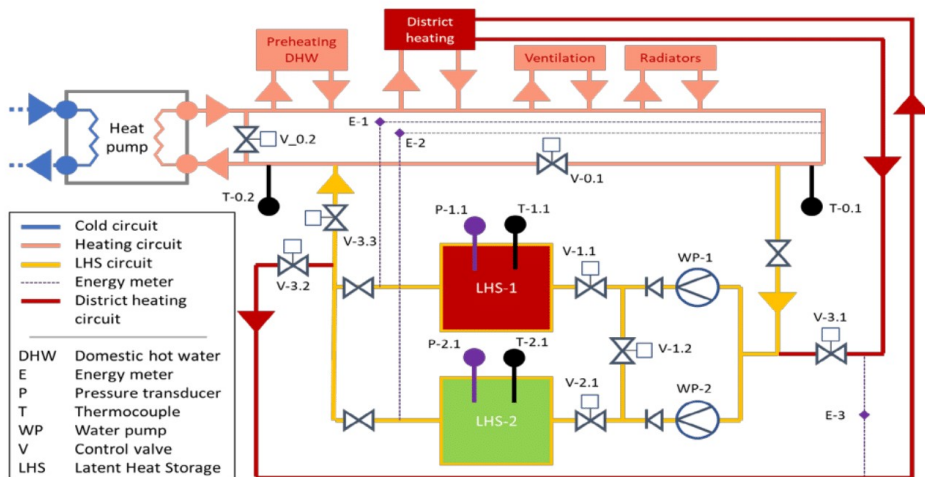


**Figure 1.** Process diagram of the centralized heating system showing the integration of the two LHS units. Only the instrumentation for control of the LHS units is shown for simplification.

Another feature available with this integration is the opportunity to use the LHS unit as a direct heat source in the building heating loop. This is meant to occur when the LHS unit is charged and the heating demand in the building is relatively low. Therefore, the heat pump can be bypassed, reducing significantly the energy use during these low-demand periods. This operational mode is especially interesting if energy price is integrated in the control system of the overall heating system.

As shown in Figure 1, the system allows for a variety of control strategies through a large number of control valves and two regulated water pumps. The selected strategy includes two levels: (1) a temperature-controlled strategy for charging and discharging using only the heat pump as heat source and heat sink; (2) a price-controlled strategy where the energy price is taken into account to decide when to harvest heat from the district heating network and when to use the LHS unit as direct heat sources for the building heating circuit. In both cases, the energy level of the LHS units is followed up using thermocouples located at various locations in the unit. Full charge is indicated by an average PCM temperature 4 K above its melting temperature range. Full discharge is indicated by an average PCM temperature 4 K below its solidification temperature range. In addition, three energy meters will enable to track the effect and accumulated transferred energy to follow up the thermal performance of the two units. The control system of the LHS system is to be fully integrated in the building control system, which will include a "researcher mode" to allow customizing and testing various control strategies.

### 3. Design and modelling

#### 3.1. PCM selection and performance testing

The most suitable PCM for the LHS unit should primarily have a melting temperature within 34-37 °C, which yields only a limited range of commercially available PCMs. Table 1 lists a selection of commercial PCMs with melting temperatures ranging from 34 °C to 37 °C, as well as some of their thermodynamic properties given by the manufacturers.

**Table 1.** Selection of commercially available PCMs.

<i>Product</i>	<i>Type</i>	<i>Melting point [°C]</i>	<i>Heat of fusion [kJ/kg]</i>	<i>Thermal conductivity [W/(m.K)]</i>	<i>Manufacturer</i>
E34	Eutectic	34	240	0.54	PCM Products
A36	Organic	36	217	0.18	PCM Products
L36S	Salt hydrate	36	260	0.6	TEAP
E37	Eutectic	37	213	0.54	PCM Products
A37	Organic	36	235	0.18	PCM Products
CT37	Organic	37	202	0.24	CrodaTherm
PCM37	Organic	37	215	N/A	Microtek

After investigation of the pre-selected commercial PCMs listed in Table 1 for the melting temperature range 34-37 °C, the PCM CrodaTherm 37 (CT37) was selected. CT37 is a water-insoluble organic PCM, derived from plant-based feedstocks [9]. The PCM appears as a crystalline wax in solid state and oily liquid above melting temperature. The main arguments in favour of this PCM are its low degree of supercooling (cf. Table 2), its low-carbon footprint as well as its affordable cost. In addition, CT37 has low flammability, which is an essential criterion in buildings.

A sample of CT37 received by CrodaTherm was analysed by TGA/DSC at the SINTEF Energy Laboratory to evaluate the thermodynamic performance of the PCM. A measurement of 10 melting/solidification cycles was performed using a Digital Scanning Calorimetry (DSC) device, with controlled heating and cooling rates of 1 K/min ranging from 30 °C to 50 °C, in a nitrogen atmosphere. The results are shown in Figure 2. As indicated by the manufacturer, the first melting displays a significantly larger latent heat of fusion than the following melting/solidification cycles. Taking into account only the 9 following cycles, CT37 remains absolutely stable, yielding very similar heat flow patterns. The average latent heat of fusion is 198.6 kJ/kg (+/- 0.9 %) and the average latent heat of crystallisation is 196.4 kJ/kg (+/- 0.7 %). The average peak melting temperature peak is 36.5 °C (+/- 0.3 %) and the average solidification temperature peak is 34.5 °C (+/- 0.1 %). The weight loss is measured to 0.04 % along the first two cycles and then remains stable for the following 8 cycles.

Note that thermodynamic property measurements might be variable from one device to another and is also known to depend on the sample mass and measurement procedure.

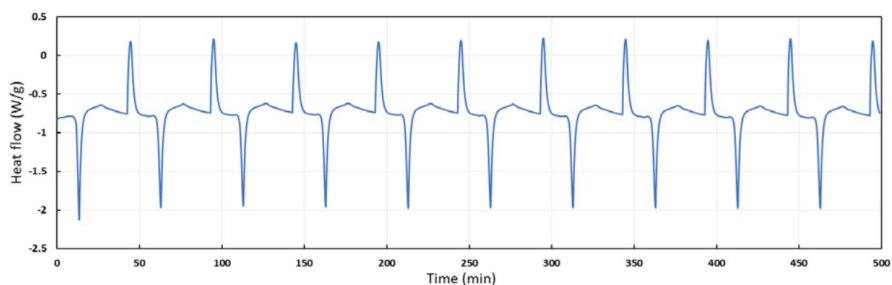


**Figure 2.** DSC measurements of heat flow absorbed and released by a sample of CT37 for 10 melting/solidification cycles.

### 3.2. General design

The general design parameter of LHS-1 are given in Table 2. The LHS unit dimensions are the first constraints to consider for the unit design due to the architecture of the building, limiting the access into the technical room through a 1.8-m wide corridor. This justifies the idea of having two LHS units whose dimensions allow to enter the building (see Table 2). The design of LHS-1, shown in Figure 3, is based on a fin-and-tube heat exchanger, filled with PCM. Water from the heating circuit circulates in the tubes. The design parameters of the fin-and-tubes heat exchanger are discussed in Section 4. Headers at both ends of the unit enable a homogeneous distribution of the water across the tubes. A thick thermal insulation around the LHS-unit allows for a theoretical heat loss under 2 % per 24 h.

**Table 2.** General design parameters of LHS-1 using a fin-and-tube heat exchanger design.

<i>Properties of LHS-1</i>	<i>Values</i>
Dimensions of LHS-1 unit (height x width x length) [m]	1.5 – 1.4 – 2.5
Measured PCM melting temperature range and peak [ $^{\circ}\text{C}$ ]	35 – 39 (36.5)
Measured PCM solidification temperature range and peak [ $^{\circ}\text{C}$ ]	33 – 35.5 (34.5)
Measured PCM latent heat of fusion [kJ/kg]	198.6
Measured PCM latent heat of crystallisation [kJ/kg]	196.4
PCM density [ $\text{kg}/\text{m}^3$ ]	957 (at $32^{\circ}\text{C}$ ), 819 (at $75^{\circ}\text{C}$ )
PCM thermal conductivity [ $\text{W}/(\text{m}\cdot\text{K})$ ]	0.24
PCM specific heat capacity (solid – liquid) [kJ/(kg.K)]	2.3 – 1.4
PCM degradation temperature [ $^{\circ}\text{C}$ ]	> 50
Total theoretical thermal storage capacity [from 30 to 40 $^{\circ}\text{C}$ ] [kWh]	325
Ratio of latent heat to total heat storage capacity	90 %

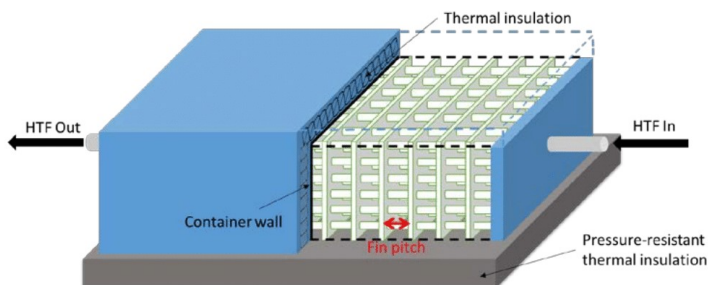


**Figure 3.** Simplified geometry of the LHS unit. The PCM (not shown here) will occupy the space between the plate fins.

---

## 4. Dynamic system modelling

### 4.1. Model description and assumptions

To investigate the transient nature of the charging and discharging processes of the LHS unit, a heat exchanger model using PCM for heat storage has been developed in the modelling and simulation software Dymola [10]. Dymola allows dynamic modelling of thermal systems with variable inputs. It is based on the open, object-oriented modelling language Modelica [6]. The specific heat exchanger model was developed using existing TIL libraries from expert thermodynamic model developers at TLK-Thermo GmbH [11]. The model is based on a solid-liquid fin-and-tube heat exchanger using PCM for TES custom-made by TLK-Thermo GmbH in 2017 and utilised in previous works [12]. This LHS model is unique as it only has one mass flow, for the heat transfer fluid (HTF), water here. The model requires the following input parameters: heat exchanger basic geometry, fin geometry, HTF inlet temperature, HTF mass flow rate, PCM and material properties, as well as the initial temperature for respectively the HTF, PCM and the heat exchanger.

The LHS model consists of tubes and plate fins running through a tank filled with PCM. Heat transfer rates are calculated from the HTF to the PCM through the tube walls and plate fins. The dimensions of the tank are 1.5-m-high, 1.4-m-wide and 2.5-m-long. To be able to operate the LHS system during peak periods (e.g. cold days), the LHS unit should be fully charged in advance. The control strategy involves to fully charge the LHS unit during off-peak hours, typically 10 hours during the night or during warmer days since the storage capacity enable several worth of heat demand in the coldest days. The LHS model enables to evaluate the heat transfer area required to be able to fully charge the system in a predetermined number of hours, assuming a HTF inlet temperature of 40 °C as it can be delivered by the heat pump in off-peak hours. Note that this is the most critical case for charging processes since the connection to district heating enables quicker charge at 45 °C.

The following assumptions are made for the numerical simulations:

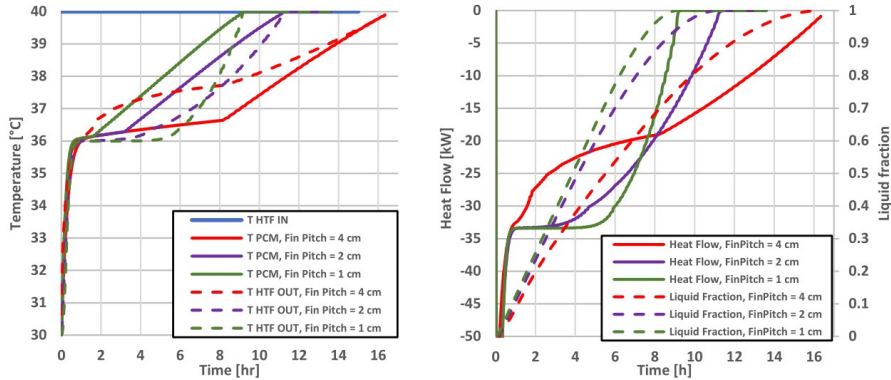
- Heat transfer coefficient between HTF and inner pipe wall are calculated using Dittus-Boelter correlation [13].
- Hysteresis effects are not accounted for in the PCM.
- No heat loss through tank wall.
- The PCM phase changes are complete during charging/discharging processes (no partial load).

Simulations are carried out for six different scenarios for both charging and discharging processes. Three scenarios are simulated with fin pitches of, respectively, 1, 2 and 4 cm, in the heat exchanger geometry for a constant HTF mass flow of 2 kg/s. The next three scenarios are simulated with a variable HTF mass flow of respectively 1, 2 and 3 kg/s, for a constant fin pitch of 2 cm. The heat exchanger consists of 225 pipes, arranged 15 x 15 across a transversal section, along the longitudinal axis, with 1 cm inner diameter. Fin thickness is set to 1 mm. The simulations are performed over a sufficiently long time period to allow for complete melting or solidification of the PCM. For the charging processes, the initial temperature is 30 °C in the whole LHS unit and the HTF inlet temperature is 40 °C. For the discharging processes, the initial temperature is 40 °C for the whole LHS unit and the HTF inlet temperature is 30 °C.

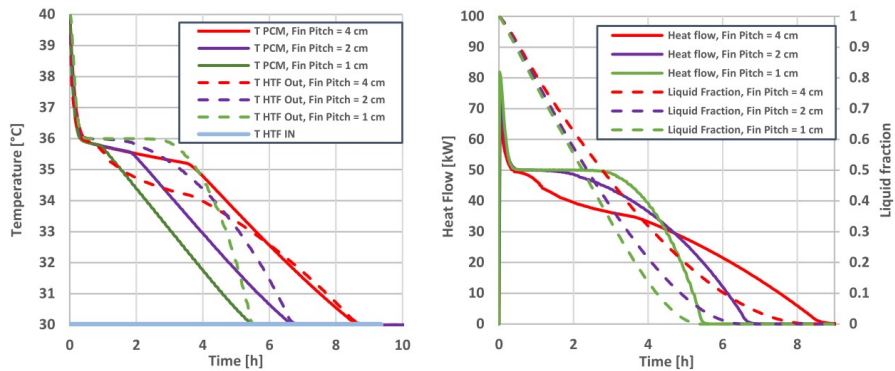
### 4.2. Results and discussion

Figure 4 shows the simulation results for one charging process with the tested fin pitches. Figure 4 (a) shows the average PCM temperature throughout the LHS unit. The charging or discharging time is defined here as the time required for the average temperature of the PCM in the LHS unit to reach the HTF inlet temperature. By reducing the fin pitch from 4 cm to 1 cm, the charging time is reduced from ca. 16 h to 9 h. This is mainly because of the increased surface heat transfer area from the increased quantity of fins, and because the shorter fin pitch also reduces the PCM volume in the LHS unit by 7 %. Figure 4 (b) shows the PCM liquid fraction and heat flow from the PCM to the HTF during the

melting process. Heat transfer flows are initially high due to the larger temperature differences driving the heat transfer. They rapidly decrease within the sensible heat transfer region, until the heat flows stabilise when reaching the latent heat transfer region for fin pitches of 1 cm and 2 cm. The fin pitch of 4 cm does not yield such a sharp change during phase change.



**Figure 4.** Charging process for various fin pitch with constant HTF mass flow of 2 kg/s, (Left) Temperature of HTF at inlet and outlet, and average PCM temperature; (Right) PCM liquid fraction and heat flow from PCM to HTF.



**Figure 5.** Discharging process for various fin pitches with constant HTF mass flow of 2 kg/s, (Left) Temperature of HTF at inlet and outlet, and average PCM temperature; (Right) PCM liquid fraction and heat flow from PCM to HTF.

Figure 5 shows the results of the discharging simulations for the tested fin pitches. As shown in Figure 5 (a), a fin pitch of 1 cm yields an HTF outlet temperature almost constant at 36 °C for 2 hours, which is optimal for the steady operation of the heat pump. Increasing the fin pitch results in steadily decreasing HTF outlet temperature during discharging. Figure 5 (b) shows that reducing the fin pitch provides higher and more constant heat flows in the latent heat transfer region, ultimately leading to shorter discharging times. According to the simulations, a fully charged system stores respectively 293 kWh, 286 kWh and 271 kWh for a fin pitch of 4 cm, 2 cm and 1 cm. This yields average heat transfer rates of ca. 35 kW, 44 kW and 50 kW for the various fin pitch distances during discharge.

These results validate the thermal performance for the proposed design of the LHS system, both in terms of charging times and heat transfer rates during discharge. Charging of the system may occur over night when the building is not in use, typically for a time period of maximum 10 hours. Figure 4 (a) shows that this can be achieved using a fin pitch distance of 1 or 2 cm. Figure 5 (a) confirms that the

---

LHS unit can raise the return temperature of the heating circuit closer to design intake conditions for the heat pump (35 °C). Figure 5 (b) demonstrates that the LHS unit is able to deliver more than sufficient heat transfer rates, to meet the maximum heat demand in combination with the heat pump.

## 5. Conclusion

The aim of the present study is to evaluate the integration and design strategies for a LHS unit to be implemented in the centralized heating system of the ZEB Flexible Laboratory building in Trondheim (Norway). The LHS unit is designed based on a fin-and-tube heat exchanger filled with PCM whose phase change temperature is 35-37 °C. Using dynamical system simulations, the thermal performance of the proposed LHS design has been evaluated. The simulated LHS unit can store close to 300 kWh and simultaneously achieve sufficiently high heat transfer rates during discharge to successfully back up the heat pump during the coldest winter days.

## Acknowledgements

The current study was carried out through the competence-building project PCM-Eff supported by SINTEF Energy Research using basic funding from the Research Council of Norway. The project aims at investigating novel phase change material solutions for efficient thermal energy storage at low and medium-high temperature ([www.sintef.no/en/projects/pcm-eff/](http://www.sintef.no/en/projects/pcm-eff/)). The LHS unit is co-financed through the ZEB Flexible Laboratory by SINTEF, NTNU, the Research Council of Norway and ENOVA.

## References

- [1] Time, B., et al. *ZEB Laboratories – Research Possibilities*. in *Proc. of NORDIC ZEB+ - 1st Nordic Conf. on Zero Emission and Plus Energy Buildings – 6-7 Nov. 2019, Trondheim (Norway)*.
- [2] Shukla, A., D. Buddhi, and R.L. Sawhney, *Thermal cycling test of few selected inorganic and organic phase change materials*. *Renewable Energy*, 2008. **33**(12): p. 2606-2614.
- [3] Sevault, A., et al., *Phase change materials for thermal energy storage in low- and high-temperature applications: a state-of-the-art*, *SINTEF Energy Research Report TR A7638 - ISBN 978-82-594-3684-9*. 2017.
- [4] Hirmiz, R., et al., *Performance of heat pump integrated phase change material thermal storage for electric load shifting in building demand side management*. *Energy and Buildings*, 2019. **190**: p. 103-118.
- [5] Jokiel, M., et al. *Phase change material thermal energy storage for a large scale ammonia chiller/heat pump system*. in *7th Conference on Ammonia and CO2 Refrigeration Technology. Proceedings: Ohrid, Macedonia, Mai 11-13, 2017*. 2017. International Institute of Refrigeration.
- [6] *Modelica and the Modelica Association - Modelica*. 2019 [Visited 2019; Available from: <https://modelica.org/>].
- [7] Bonamente, E., A. Aquino, and F. Cotana, *A PCM Thermal Storage for GSHP: Simulating the System Performance via CFD Approach*. *Energy Procedia*, 2016. **101**: p. 1079-1086.
- [8] Moreno, P., et al., *PCM thermal energy storage tanks in heat pump system for space cooling*. *Energy and Buildings*, 2014. **82**: p. 399-405.
- [9] *Crodatherm 37 - Datasheet*, C.I. Plc, Editor. Consulted in May 2019.
- [10] *Dassault Systèmes - DYMOLA Systems Engineering* 2019 [Visited 2019; Available from: <https://www.3ds.com/products-services/catia/products/dymola/>].
- [11] *TLK-Thermo GmbH, TIL Suite Thermal Systems*. 2019 [Visited 2019; Available from: <https://www.tlk-thermo.com/index.php/en/software-products/til-suite>].
- [12] Jokiel, M., et al., *Dynamic modelling of a refrigerated cabinet with integrated phase change material thermal storage*. *Proceedings of the 25th International Congress of Refrigeration*, August 24-30, Montreal (Canada), 2019.
- [13] Dittus, F.W. and L.M.K. Boelter, *Heat transfer in automobile radiators of the tubular type*. *International Communications in Heat and Mass Transfer*, 1985. **12**(1): p. 3-22.

---

## C Matlab script for heat transfer coefficient calculations

Matlab script for calculating heat transfer coefficient for HTF.

```
clc
clear all
%%
d=0.01; %PIPE DIAMETER
m_in=[2]; % MASS FLOW
n_pipe=225; %NUMBER OF PIPES
para=linspace(1,225,225);% Number of separate flows

%% Properties of water at 35C
mu=733E-6; %Dynamic viscosity
k=0.62; %Thermal conductivity
Pr=(4086*mu)/k; %Prandtl number
n1=0.3;

for i=1:1:225
m=m_in/i;
Re=(4*m)/(pi*m*d); %Reynolds number
if Re>=2300 %Assuming turbulent flow for Re>2300
Nu_c(i)= 0.023*(Re.^0.8)*(Pr.^n1); %Dittus-Boelter correlation for heat transfer in circular
pipe flow
h_charging(i)=(Nu_c(i)*k)/d;
else if Re<2000
Nu_c(i)= 3.66;
h_charging(i)=(Nu_c(i)*k)/d;
end
end
end

plot(para,h_charging,'Linewidth',2)
axis([0 225 10 100000])
ax=gca;
set(gca, 'Yscale', 'log')
curtick = get(gca, 'YTick');
set(gca, 'YTickLabel', cellstr(num2str(curtick(:))))
xticks([linspace(0,225,16)])
xlabel('Number of separate flows')
ylabel('Heat transfer coefficient [W/m^2K]')
```



---

## D Matlab script for pressure drop calculations

Matlab script for calculating pressure drop for HTF.

```
clc
clear all
%%
d=0.01; %Pipe diameter
m_in=2; % Mass flow
n_pipe=225; %Number of pipes
n_flow=linspace(1,225,225); %
A=pi*0.25*(d^2);
%%%%%%%%%%%%%%%%%%%%%%%%%%%%%%%%%%%%%%%%%%%%%%%%%%%%%%%%%%%%%%%%%%%%%%%%Properties of water%
rho=1000;|
e=0.0015;
k=0.62;
mu=733E-6;
%%%%%%%%%%%%%%%%%%%%%%%%%%%%%%%%%%%%%%%%%%%%%%%%%%%%%%%%%%%%%%%%%%%%%%%%
m=m_in./n_flow; %Mass flow in each tube
v=m/(rho*A); %HTF velocity
Pr=(4086*mu)/k; %Prandtl Number
L=(n_pipe./n_flow)*2.5; %Pipe length for each separate flow
Re=(4.*m)./(pi*mu*d);

%FRICTION FACTOR SWAMEE-JAIN EQUATION
a=(0.3086*(3^2));
b=( log( ((7.7./Re).^3) + (e/(3.7*d))^(1.11*3) ) ).^2;
f=a./b;

z=zeros(1,length(b)); %Modelica results
z(1)=2832; z(2)=387; z(3)=121; z(4)=54; z(5)=28.8; z(6)=17.25;
z(7)=11.2; z(8)=7.71; z(9)=5.55; z(10)=4.13; z(11)=3.17; z(12)=2.5;
z(13)=2; z(14)=1.62; z(15)=1.34; z(16)=1.12;

%Pressure Drop for straight section and for 180 degree bends
dp=f.*(L/d)*(rho/2).*(v.^2); %Pressure drop in tubes
bp=f.*(pi*0.05)/d*(rho/2).*(v.^2)+(rho/2).*(v.^2)*0.3; %Pressure drop bends
nbends=n_pipe-n_flow;
dp_bar=dp/100000;

%PRESSURE DROP HEADER
dp_entrance=(0.5.*(v.^2)*1/(2*9.81))*10.2; %10.2 = head to pressure
dp_exit=((v.^2)*1/(2*9.81))*10.2; %10.2 = head to pressure
dp_pipes=(dp+bp.*nbends)/100000;
dp_tot=dp_pipes+dp_entrance+dp_exit; %Including bends and headers assuming k=0.5 for entrance
a

figure(1)
plot(n_flow(1:25),dp_tot(1:25),n_flow(1:25),dp_bar(1:25),n_flow(1:25),z(1:25),'x','MarkerSize'
,10,...
'MarkerEdgeColor','black','Linewidth',2)
ax=gca;
set(gca, 'yscale', 'log')
curtick = get(gca, 'YTick');
set(gca, 'YTickLabel', cellstr(num2str(curtick(:))))
xlabel('Number of separate flows')
ylabel('dp [bar]')
legend('Total pressure drop','HTF tube pressure drop (without bends)','simulated pressure
drop')
grid on
```

---

## E Matlab script for LHS unit heat loss

Matlab script for heat loss calculation through LHS unit walls.

```
k1c
clear all

%Thermal properties of steel and insulation
k_ins=0.04;
k_steel=50.2;

t_steel=0.003; %Thickness of container wall
A=18.7; %Container wall area
Tw=40; %LHS unit temperature charged
TcW=30; %LHS unit temperature discharged
Tins=15; %Surrounding temperature
h=22; %Heat transfer coefficient surrounding air (free convection)

t_ins=linspace(0,0.3,21000);
R_tot=((t_steel/k_steel)+(t_ins/k_ins)+(1/h));

dTh=Tw-Tins;
dTc=TcW-Tins;
R_ins=(t_ins/k_ins)+(1/20);
q =- A*dTh./(R_tot);
q_cold=-A*dTc./(R_tot);

plot(t_ins,q,t_ins,q_cold)
axis([0 0.3 -1000 0])
xlabel('Insulation thickness [m]')
ylabel('Heat loss [W]')
legend('charged','discharged')
```